Locomotor Compensation for Severe Motor Neuron Loss during Amyotrophic Lateral Sclerosis Disease Progression

by

Lauren Marie Landoni

Submitted in partial fulfillment of the requirements

for the degree of Master of Science

at

Dalhousie University

Halifax, Nova Scotia

December 2016

To Mom and Dad,
Thank you for always encouraging me to follow my dreams
and for giving me the love and support to see them to fulfillment.
It means the world to me.

Table of Contents

List of Figures

Abstract

Amyotrophic lateral sclerosis (ALS) causes progressive motor neuron (MN) degeneration leading to muscle weakness, paralysis, and eventually death. When symptoms are detected in ALS patients and model animals ($SOD1^{G93A}$ mice) large motor unit loss has occurred, indicating existence of a compensatory mechanism that masks denervation. Although significant denervation has occurred by P90 in $SOD1^{G93A}$ mice, motor disturbances are minimal. Cholinergic modulation of MNs through the C-boutons was hypothesized to compensate for motor unit loss by increasing the excitability of surviving MNs. After P100, $V0_C$ interneurons, the neuronal source of C-boutons, became active during walking in $SOD1^{G93A}$ mice and the ability to upregulate gastrocnemius activity during swimming became impaired. Silencing of the C-boutons in $SOD1^{G93A}$ mice caused earlier changes in gait and deficits in ankle range of motion. Based on these observations, targeting C-bouton activation using exercise or pharmacological therapies could improve quality of life in ALS patients by preserving mobility.

List of Abbreviations and Symbols Used

~	Approximately
^{o}C	Degree Celsius
>	Greater than
≥	Greater than or equal to
%	Percent
±	Plus or minus
ACh	Acetylcholine
ALS	Amyotrophic lateral sclerosis
cm	centimeter
ChAT	Choline acetyl transferase
CMAP	Compound muscle action potential
EMG	Electromyogram
fALS	Familial ALS
FF	Fast fatigable motor unit
FR	Fast fatigue-resistant motor unit
fl	floxed
Gs	Gastrocnemius
kHz	kilohertz
kg	kilogram
L2	lumbar spinal cord segment 2
L3	lumbar spinal cord segment 3
L4	lumbar spinal cord segment 4

L5	lumbar spinal cord segment 5
m/s	meters per second
μA	microampere
μl	microliter
mg	milligram
ml	milliliter
mm	millimeter
MUNE	Motor unit number estimation
NMJ	Neuromuscular junction
PBS	Phosphate buffered saline
PBST	PBS with Triton X-100
PFA	Paraformaldehyde
ROM	Range of Motion
S	Slow motor unit
sALS	Sporadic ALS
SD	Standard deviation
SK	Calcium-dependent potassium channel
SOD1	Superoxide dismutase 1
Sol	Soleus
TA	Tibialis anterior
V0$_C$	V0 cholinergic
VAChT	Vesicular acetylcholine transporter
WT	Wildtype

Acknowledgements

First, thank you to my supervisor, Dr. Turgay Akay, for your support, encouragement, and advice over the years. You accepted me into the lab even though I had no prior research experience and I am very grateful for all of the knowledge and skills that I have learned from you. Thank you for encouraging me to think critically, for indulging my sometimes far-fetched theories, and for laughing at my very bad jokes. Your encouragement and enthusiasm for research have been truly inspiring and it has been a privilege to be in your lab.

Thank you to my supervisory committee, Dr. Victor Rafuse, Dr. Ying Zhang, and Dr. George Robertson for all of your time, guidance, and advice over the last couple of years. Your unique perspectives and backgrounds have taught me to view my data in new ways and pursue new avenues and for that I am thankful.

To Brenda Ross, my technician, my lab mom, and my very first friend in Halifax, thank you for the countless hours that you have spent teaching me and helping me develop my technical skill set. You are always looking out for me, encouraging me, and believing in me. Your kindness, goofiness, and perpetual love for fun has made my time here so enjoyable and I will never forget it.

To my colleagues, William Mayer and Olivier D Laflamme, I am very fortunate to also be able to call you my friends. You have been incredibly supportive over the last couple of years and you make the lab a great place to be. Thank you for always helping me troubleshoot my problems and letting me bounce ideas off of you. And yes, I am still the boss. Even when I leave.

To the many friends that I have made during my time in Halifax, you bring so much joy to my life. Stephanie Blandford, Kaitlyn Keller, and Julia Harrison, I could not have done this without you. Thank you for being the best friends and support system I could have ever asked for, thank you for making me laugh until I cry, and thank you for all of the amazing memories.

To my bigger, cooler older brothers, Matt and Nick, I think it is safe to say that you have made me resilient. It turns out that is an important quality in science, so thank you. Thank you for letting me vent, cheering me up, and for always believing in me and pushing me. To Uncle Timmy and Aunt Vicky, thank you for my home away from home. I am very grateful for everything that you have done for me. To Markus Venturato, thank you for the overwhelming support, love, and happiness throughout this journey. Thank you for reading my thesis and letting me babble on about science even though you are an accountant and have no idea what I am talking about.

CHAPTER 1: INTRODUCTION

Amyotrophic lateral sclerosis (ALS) is an adult-onset neurodegenerative disease characterized by the progressive death of cortical and spinal motor neurons. Motor neuron death leads to muscle weakness, paralysis, and eventually death due to denervation of the respiratory muscles (Cleveland & Rothstein, 2001). Approximately 90% of ALS cases occur sporadically with no known genetic linkage (sALS) while only ~10% of ALS cases have a familial origin (fALS) (Pasinelli & Brown, 2006). Of the 10% of ALS cases that are familial, 20% have been linked to a mutation in the superoxide dismutase 1 (SOD1) gene (Boillée et al., 2006). To gain a greater understanding of ALS disease progression, several animal models of ALS have been developed.

Mutant forms of human SOD1 (most commonly $SOD1^{G93A}$) have been overexpressed in mice to generate animal models of ALS that mimic disease progression in terms of selective loss of motor neurons and development of muscle weakness and paralysis (Gurney et al., 1994). Although many important insights into the sequence of changes and pathological mechanisms of ALS have been elucidated using the $SOD1^{G93A}$ mice, comprehensive investigations of disease progression at a physiological and behavioural level are limited (Akay, 2014; Tysseling et al., 2013).

There are no effective treatments or therapies for ALS that markedly improve motor function, survival, or quality of life. When patients begin experiencing changes in muscle strength and seek medical care they have already lost up to 50% of their motor units (McComas, Sica, Campbell, & Upton, 1971; van Dijk et al., 2010). The significant loss of motor units prior to diagnosis represents both a difficulty to diagnose the disease and the existence of a compensatory mechanism that masks symptoms of motor unit loss. The mechanism underlying compensation has been scarcely

investigated and represents a potential therapeutic target for improving mobility and quality of life. Therefore, the objectives of the present study were to: 1) Determine the approximate timeline of muscle denervation in the high-expresser SOD1^{G93A} mouse line, 2) Longitudinally examine the *in vivo* physiological and behavioural changes in individual SOD1^{G93A} mice throughout ALS disease progression, 3) Identify a potential compensatory mechanism that allows SOD1^{G93A} mice to produce asymptomatic movements despite established loss of motor units. Characterization of the compensatory mechanism will provide new directions to pursue for of ALS treatments that will improve patient mobility and quality of life.

1.1 Introduction to Amyotrophic Lateral Sclerosis

The most common motor neuron disease in human adults is ALS (Nardo et al., 2016). ALS affects approximately two in every 100,000 people per year, with males being affected more frequently than females (Robberecht & Philips, 2013). The clinical onset of ALS is typically between 40 and 70 years of age (biological onset may occur at earlier ages) with death occurring approximately two to five years after symptom onset (Robberecht & Philips, 2013). ALS onset occurs most often in the limb muscles and the earliest observable symptoms are reduced dexterity, fasciculations, and stumbling during walking. Alternatively, ~25% of cases have bulbar onset in which the muscles for speech and swallowing are affected first (Kiernan et al., 2011). With the progressive loss of motor neurons, muscles become increasingly weak and begin to atrophy, eventually resulting in paralysis. At later stages of ALS, the paralysis becomes so severe that patients are no longer able to independently walk, speak, eat, or breathe (Bansal, Singhvi, & Rajpurohit, 2015). There is no cure for ALS, and therapies that substantially alleviate symptoms

in patients are lacking. Discovery of the underlying mechanism of ALS pathogenesis is imperative to the development of treatments that will effectively treat symptoms and potentially cure ALS.

1.2 Motor Pathology in Amyotrophic Lateral Sclerosis

Genetic mutations identified in human cases of ALS led to the development of animal models of ALS that express mutated human fALS genes. Several animal models have been developed that accurately recapitulate many of the symptomatic and pathophysiological characteristics of ALS observed in humans. The study of these models using histological, *in vitro* and *in vivo* physiological, and behavioural techniques has yielded a considerable amount of information regarding ALS disease progression. The majority of this information has been uncovered through study of the $SOD1^{G93A}$ mouse model of ALS.

1.2.1 The $SOD1^{G93A}$ Mouse Model of ALS

The $SOD1^{G93A}$ mouse is the most widely used animal model of ALS disease progression (Hegedus, Putman, & Gordon, 2007). The $SOD1^{G93A}$ mouse overexpresses a mutant form of the Cu/Zn superoxide dismutase 1 (SOD1) gene that accounts for 20% of human fALS cases (Boillée et al., 2006). $SOD1^{G93A}$ mice develop progressive motor neuron degeneration, muscle weakness, and eventual paralysis which are due to a toxic gain-of-function rather than a loss-of-function of SOD1 enzymatic activity (Chiu et al., 1995; Pasinelli & Brown, 2006). Importantly, the onset and rate of disease progression in $SOD1^{G93A}$ mice is dependent on the number of transgene copies expressed (Gurney et al., 1994) and the genetic background of the mice (Nardo et al., 2016). There is also variability in the phenotype of $SOD1^{G93A}$ mice between laboratories using identical strains (Kanning, Kaplan, & Henderson, 2010). These factors, combined with inconsistency in the method

of characterizing disease onset makes the development of an accurate timeline of disease progression in SOD1^{G93A} mice difficult. Symptom onset is largely reported to occur at ~P90 (Chiu et al., 1995; Fischer et al., 2004; Gurney et al., 1994; Hegedus et al., 2007), however other studies report symptom onset closer to P60 (Gerber, Sabourin, Rabano, Vivanco, & Perrin, 2012; Mancuso, Oliván, Osta, & Navarro, 2011; Mead et al., 2011). Progressive paralysis begins to occur in this model at ~P120 and rapidly progresses until animals reach end-stage at ~P140 (Vinsant, Mansfield, Jimenez-Moreno, Del, et al., 2013). The use of the SOD1^{G93A} mouse model has yielded a large amount of information relating to the cellular and physiological changes that occur with ALS disease progression.

1.2.2 Histological Analysis of Denervation and Motor Neuron Death in SOD1^{G93A} Mice

During ALS disease progression, the ability to move becomes progressively impaired due to muscle weakness and wasting caused by pathological changes to motor neurons and central nervous system support cells (Di Giorgio, Carrasco, Siao, Maniatis, & Eggan, 2007; Nagai et al., 2007). Movements are produced by transmitting a motor command from the motor neuron to the effector muscle and causing its contraction. The neuromuscular junction (NMJ) is a chemical synapse where the presynaptic motor axon terminal and motor end plates on the post-synaptic muscle fiber interact. At the NMJ, acetylcholine (ACh) is released by the motor axon terminal and traverses the synaptic cleft to bind to nicotinic ACh receptors on muscle fibers to cause a muscle contraction (Sanes & Lichtman, 1999). The motor deficits associated with disease progression in SOD1^{G93A} mice were once thought to result from motor neuron death, but mounting evidence suggests that motor deficits are actually caused by dying back of the motor neuron from the NMJ rather than death of the motor neuron itself (Fischer et al., 2004; Frey et al., 2000). Histological

analysis of NMJ innervation has shown that denervation (withdrawal of the motor neuron from the NMJ) occurs in SOD1^{G93A} mice as early as ~P50 (Fischer et al., 2004; Frey et al., 2000; Pun, Santos, Saxena, Xu, & Caroni, 2006). Severe loss of motor axons from the ventral root is observed at ~P50-80, followed by loss of motor neuron cell bodies from the lumbar spinal cord after P80 (Fischer et al., 2004; Kanning et al., 2010). Total motor neuron loss in the lumbar spinal cord of SOD1^{G93A} mice is ~50% by end-stage of the disease (Vinsant, Mansfield, Jimenez-Moreno, Moore, et al., 2013). This histological progression of motor neuron degeneration from proximal to distal supports the hypothesis that motor dysfunction in ALS is caused by dying back of the motor neuron rather than motor neuron death itself. When motor neuron death is completely prevented by knocking out the pro-apoptotic gene, Bax, denervation, though delayed, still occurred in SOD1^{G93A} mice (Gould et al., 2006). Dying back of motor neurons during ALS disease progression does not occur uniformly in all motor neurons. Rather, certain motor neuron subtypes and their motor units are more susceptible to denervation and degeneration at different disease stages.

A motor unit is one motor neuron and all of the skeletal muscle fibers that it innervates. There are three different subtypes of motor units: slow-twitch (S) units, fast-twitch fatigue-resistant (FR) units, and fast-twitch fatigable (FF) units (Burke, 1967). Type S motor units have motor neurons with small, easily depolarized cell bodies and axons that control type I muscle fibers (Burke, Levine, Tsairis, & Zajac, 1973). Type I muscle fibers have a slow twitch and use aerobic respiration for energy, making them resistant to fatigue. As a whole, type S motor units produce small contractions and have slower fatigue-resistant firing rates that are ideal for performing movements requiring small, sustained contractions (e.g., maintenance of posture) (Burke, Levine, Zajac, Tsairis, & Engel, 1971; Burke, 1980). Type FR and FF motor units have motor neurons

with large cell bodies and axons that control type IIa and type IIb muscle fibers, respectively (Burke et al., 1971). Type IIa and IIb muscle fibers both have a fast twitch but differ in their sources of energy and therefore fatigability. Type IIa muscle fibers use aerobic and anaerobic respiration, providing them with an intermediate resistance to fatigue. In contrast, type IIb muscle fibers rely primarily on anaerobic respiration, making them susceptible to fatigue (Edstrom & Kugelberg, 1968). Both type FR and FF motor units have faster firing rates than type S motor units, and produce larger amounts of force ideal for fast, powerful contractions (Burke, 1980). Type FR motor units have more intermediate properties than type FF and are resistant to fatigue, while type FF motor units are easily fatigued (Edstrom & Kugelberg, 1968). These differences in size, firing properties, and metabolic demands cause certain motor units to be more susceptible to ALS.

The FF motor units are the first to be affected by ALS, followed by FR motor units and then S motor units (Frey et al., 2000). The gastrocnemius (Gs) and tibialis anterior (TA) muscles are composed predominantly of FF and FR motor units and are among the first muscles affected in $SOD1^{G93A}$ mice. In the Gs muscle of $SOD1^{G93A}$ mice at ~P60, 78% of type IIb muscle fibers have been denervated by FF motor neuron terminals, 22% of type IIa muscle fibers have been denervated by FR motor neurons, and 0% of type I muscles fibers have been denervated by S motor neurons (Frey et al., 2000). Total denervation of the Gs muscle at P60 was reported to be ~60% (Mead et al., 2011). In the TA muscle, Vinsant et al. found that total denervation is ~40% at P30 and reaches 70% by P100. In contrast, they found no denervation of the slow-twitch soleus muscle at P30 and only a slight, insignificant increase in denervation above WT at P100 (Vinsant, Mansfield, Jimenez-Moreno, Moore, et al., 2013). Overall, analysis of NMJ innervation in $SOD1^{G93A}$ mice using immunohistochemistry has demonstrated that muscle denervation during

ALS disease progression is dictated by motor unit type with FF and FR motor units being particularly susceptible, whereas S motor units are relatively resilient.

1.2.3 Denervation Estimates using Electromyography in SOD1^{G93A} Mice

In addition to immunohistochemistry, electromyography tests have been used to quantitatively investigate motor unit loss in SOD1^{G93A} mice. The compound muscle action potential (CMAP) is a neurophysiological measure that reflects muscle fiber innervation (Maathuis, Drenthen, Van Doorn, Visser, & Blok, 2013). During a muscular contraction, motor units are recruited based on the Henneman size principle which describes the early recruitment of small motor units that produce low force followed by the later recruitment of larger motor units that produce higher force. According to the size principle, motor units are recruited from Type S → Type FR → Type FF (Henneman, 1957). The CMAP is calculated by stimulating a nerve upstream of the muscle of interest at gradually increasing intensities from subthreshold to supramaximal values to activate all possible motor units. As peripheral nerves contain motor and sensory axons, stimulation of the nerve generates an action potential in both motor neurons which travels distally to the muscles and in group Ia proprioceptive afferents which travels to the spinal cord (Akay, 2014). The distally travelling action potential in the motor neuron excites muscle fibers and is captured in the electromyogram (EMG) recordings as the M-wave. The action potential in the proprioceptive afferents travels to the spinal cord and excites homonymous motor neurons through largely mono-synaptic connections, generating a second more delayed response at the muscle that is captured as the H-wave (Zehr, 2002). CMAP changes can be used to monitor denervation in SOD1^{G93A} mice by inferring that decreases in the CMAP indicate net denervation of the muscle or a loss of activatable motor units (Maathuis et al., 2013).

Analysis of CMAP changes during ALS disease progression in individual mice has been performed using a chronically implanted tibial nerve stimulation cuff and recording EMG electrodes in the Gs and Sol muscles (Akay, 2014). Using this method, it was shown that average Gs and Sol CMAP values were significantly lower in SOD1^{G93A} mice comparted to WT mice at almost all ages recorded. Gs CMAP values were shown to decline drastically in SOD1^{G93A} mice as the disease progressed while Sol CMAP values remained relatively constant throughout. Additionally, the excitability of SOD1^{G93A} motor neurons was shown to be equivalent to WT mice until P100 when motor neurons become less excitable (Akay, 2014). CMAP measurements can also be used to calculate motor unit number estimates (MUNE) by dividing the whole muscle response by the average motor unit response (Major, Hegedus, Weber, Gordon, & Jones, 2007).

Hegedus et al. assessed changes in MUNE throughout disease progression in SOD1^{G93A} mice by dividing the whole muscle isometric contractile force by the average motor unit contractile force (Hegedus et al., 2007). The Gs MUNE at P40 was ~22% lower than controls and underwent further declines at P40-60 and P80-100 followed by a plateau from P100-120. Similar to the Gs MUNE, the TA MUNE declined biphasically with a sharp decline occurring at P40-50 followed by a gradual decline that reached a plateau at P70, and a second significant decline from P80-100 followed by another plateau from P100-P120. In contrast, in the slow-twitch Sol muscle there was no difference in MUNE until P90 when the number of motor units was reduced by ~20% compared to control mice. The Sol MUNE continued to decline until P100, but also plateaued from P100-120 (Hegedus et al., 2007). Changes in muscle innervation monitored through CMAP and MUNE measurements indicate that a significant amount of denervation has occurred in fast- and slow-

twitch muscles of SOD1^{G93A} mice by P100. SOD1^{G93A} mice begin to show motor symptoms at P90 (Chiu et al., 1995) which suggests that at ~P90-100 muscle denervation has exceeded the motor system's ability to compensate for motor unit loss. As a result, SOD1^{G93A} mice begin to experience muscle tremors and changes in gait during locomotion (Akay, 2014; Chiu et al., 1995).

1.3 Locomotion

Locomotion is one of the most basic motor behaviours essential to animal survival. Locomotor behaviours are characterized by repetitive, stereotyped movements with rhythmic alternations of flexor and extensor muscles (Grillner, 1975). Walking and swimming are two common examples of locomotion. Walking depends on the ability of the nervous system to modulate the activity of multiple limb flexor and extensor muscles to produce coordinated movements of the hip, knee, and ankle joints (Grillner, 1975). Each step during walking is a cycle that can be divided into two distinct phases: swing phase and stance phase. Swing phase encompasses the time from when the foot leaves the ground and begins to move forward until it is placed back on the ground. Stance phase begins when the foot lands on the ground and the leg begins to bear weight and ends at the beginning of swing phase. Flexor muscles tend to be more active during swing phase while extensor muscles are more active during stance phase (Grillner, 1975). Gait is the manner in which stepping is performed and can be characterized by parameters such as: duration of swing and stance phase, step cycle duration, and stride length. Changes in gait occur with changes in speed, and more importantly with changes in muscle strength. Therefore, gait analysis is a useful tool for evaluating motor deficits in neuromuscular diseases such as ALS.

1.3.1 Gait Analysis in Mouse Models of ALS

Gait analysis is sensitive to subtle abnormalities in locomotion and therefore can be a useful tool for identifying early markers of disease onset in animal models of ALS, including $SOD1^{G93A}$ mice. Gait has been analyzed in $SOD1^{G93A}$ mice using multiple methods including: foot print analysis and ventral and lateral plane videos of treadmill walking. Footprint analysis and ventral plane treadmill videos all analyze paw placement during locomotion to calculate changes in gait parameters (Guillot, Asress, Richardson, Glass, & Miller, 2008; Mead et al., 2011; Wooley et al., 2005). Alternatively, gait analysis of lateral plane treadmill locomotion videos involves tracking markers identifying landmarks of interest to calculate standard gait parameters (Akay, 2014; Preisig et al., 2016; Tysseling et al., 2013). Through the use of all of these methods, several important observations have been made about locomotion changes during ALS disease progression in model mice.

$SOD1^{G93A}$ mice with muscle weakness due to motor unit loss show gait changes that involve mainly altered hind-limb movement (Preisig et al., 2016). The stance phase duration is reported to increase in $SOD1^{G93A}$ mice compared to WT mice in several studies, though the age at which this is reported is variable. A change in stance duration was reported at ~P60 in two studies (Mead et al., 2011; Wooley et al., 2005), whereas another study did not report this change until ~P90 (Mancuso et al., 2011), and one was unable to detect it at all (Guillot et al., 2008). Decreases in the stepping frequency occur at ~P90 (Mancuso et al., 2011) and stride lengths become shorter between ~P90-P120 compared to WT mice (Gurney et al., 1994; Mead et al., 2011; Preisig et al., 2016). $SOD1^{G93A}$ mice also develop fluctuations in the ankle angle during swing phase at ~P85 (Akay, 2014) and a more limited range of motion of the ankle joint beginning at ~P80 (Preisig et

al., 2016). Stability during locomotion appears to decrease at ~P85 when SOD1^{G93A} mice begin relying more on the use of three limbs to support their weight rather than diagonal limbs (Mead et al., 2011). Finally, SOD1^{G93A} mice are no longer able to walk at faster speeds (above 0.2m/s) by ~P120 (Mancuso et al., 2011). Overall, gait analysis is able to provide important information about motor performance of SOD1^{G93A} mice, but information regarding motor function can only be inferred without simultaneous analysis of muscle activity.

1.3.2 Analysis of Muscle Activity during Locomotion

To relate the changes in gait detected using kinematic analysis to changes in motor function in SOD1^{G93A} mice, simultaneous recordings of muscle activity must be performed during locomotion. Electromyography can be used to measure the changes in muscle activity that occur during locomotion due to changes in the number of motor units recruited and the firing rates of already active motor units. Until recently, locomotion was primarily studied in cats and the methods for acquiring EMG activity in freely behaving mice had not yet been developed. As a result, there are a limited number of studies that use *in vivo* EMG electrodes to investigate muscle activity during locomotion in mice (Akay, 2014; Akay et al., 2006; Akay, Tourtellotte, Arber, & Jessell, 2014; Courtine et al., 2008; Leblond, L 'Espérance, Orsal, & Rossignol, 2003; Pearson, Acharya, & Fouad, 2005; Tysseling et al., 2013). Two separate studies have applied this method in SOD1^{G93A} mice to assess its viability as a long-term *in vivo* measurement of disease progression. Tysseling et al. performed recordings in SOD1^{G93A} mice for a five-week period spanning symptom onset and demonstrated that at P100 large amplitude motor unit potentials are observed in the muscles of SOD1^{G93A} mice that were not present at earlier, pre-symptomatic stages (Tysseling et al., 2013). In the Akay, 2014 study, SOD1^{G93A} mice were implanted with EMG electrodes for up

to three months and the development of an abnormal TA activity profile was observed at ~P85 (Akay, 2014). It is important to note that these studies were not intended to comprehensively analyze the $SOD1^{G93A}$ mice, but to confirm the viability of using chronically implanted EMG electrodes as a method of monitoring changes in motor function. A detailed analysis of EMG changes during treadmill locomotion from pre-symptomatic stages through to end-stage has not been performed in $SOD1^{G93A}$ mice.

The ability of $SOD1^{G93A}$ mice to perform other locomotor tasks, such as swimming, has not been investigated. A higher output of activity from the Gs is required to propel the body through a fluid medium than is required to push off from a solid medium. As a result, the amplitude of Gs EMG activity is increased, at least in rodents, during swimming compared to walking (Hutchison, Roy, Hodgson, & Edgerton, 1989). As swimming requires a higher motor output than walking, monitoring of EMG changes in the Gs of $SOD1^{G93A}$ mice during swimming may provide important information about motor function that cannot be obtained from EMG analysis of walking alone. Muscle activity can be increased by increasing the number and size of motor units recruited or by increasing the firing frequency of motor units already active (Winter, 1990). Increases in motor neuron firing frequency can be achieved by cholinergic modulation of motor neurons through the C-boutons (Miles, Hartley, Todd, & Brownstone, 2007).

1.4 C-Boutons

C-boutons are large cholinergic terminals that synapse on the soma and proximal dendrites of motor neurons and modulate motor neuron excitability (Conradi & Skoglund, 1960). The neuronal source of C-boutons is a small subset of V0 (Dbx1+) cholinergic interneurons ($V0_C$) that express

the paired domain transcription factor Pitx2 (Zagoraiou et al., 2009). $V0_C$ interneurons are excitatory interneurons located in the vicinity of the central canal (lamina X) in the lumbar spinal cord (Huang, Noga, Carr, Fedirchuk, & Jordan, 2000; Zagoraiou et al., 2009). The C-boutons release ACh which binds to post-synaptic metabotropic m2 muscarinic receptors on motor neurons (Hellström, Oliveira, Meister, & Cullheim, 2003; Miles et al., 2007). The activation of m2 muscarinic receptors causes a reduction of the after-hyperpolarization through blockage of the calcium-dependent potassium (SK) channels clustered on post-synaptic motor neurons. Reduction of the after-hyperpolarization allows for an increase in the firing frequency of motor neurons (Deardorff et al., 2013; Miles et al., 2007; Witts, Zagoraiou, & Miles, 2014). Recently, Zagoraiou et al. silenced the C-boutons by preventing the synthesis of ACh using a conditional knock-out of the ACh biosynthesis enzyme, choline acetyltransferase (ChAT). The ability of C-bouton silenced mice to upregulate Gs activity during swimming was significantly decreased compared to WT mice (Zagoraiou et al., 2009). This finding suggests that C-boutons modulate motor neuron excitability during locomotion to produce muscular contractions of the appropriate intensity to match the demands of different motor tasks (Witts et al., 2014; Zagoraiou et al., 2009). Interestingly, changes in the C-boutons have been observed in both $SOD1^{G93A}$ mice and human ALS patients (Chang & Martin, 2009; Herron & Miles, 2012; Lasiene et al., 2016; Milan et al., 2015; Nagao, Misawa, Kato, & Hirai, 1998; Pullen & Athanasiou, 2009; Saxena et al., 2013) which suggests that C-boutons may play a role in ALS.

1.4.1 C-boutons in ALS

Observations of C-bouton changes in human cases of sALS and mouse models of ALS are morphological in nature. A loss of C-boutons on spinal motor neurons has been documented in

sALS patients at post-mortem autopsy (Nagao et al., 1998). In SOD1^{G93A} mice, variable findings regarding the size and number of C-boutons and the age at which these differences occur have been reported. Several studies have reported a significant increase in the size of C-boutons on spinal motor neurons in pre-symptomatic SOD1^{G93A} male mice at ~P20-40 compared to WT mice (Herron & Miles, 2012; Milan et al., 2015; Saxena et al., 2013). One of these studies identified a less pronounced enlargement of the C-boutons in female SOD1^{G93A} mice that occurred 8-10 days after the enlargement in males (Saxena et al., 2013). In another study, C-boutons were found to be enlarged by P70 and were further enlarged at P156 in male and female SOD1^{G93A} mice (Pullen & Athanasiou, 2009). However, C-boutons have also been reported to be significantly smaller in male SOD1^{G93A} mice at P100 (Milan et al., 2015) and SOD1^{G93A} mice are reported to have significantly fewer C-boutons per motor neuron at P120-P150 than WT mice (Chang & Martin, 2009; Lasiene et al., 2016). Overall, in SOD1^{G93A} mice it appears as though C-boutons are enlarged in the pre-symptomatic stages of ALS and remain enlarged until at least P100 then possibly withdraw from motor neurons or degenerate at P120-P150. The observed changes in the C-bouton system during ALS disease progression in conjunction with previous knowledge that C-boutons modulate motor neuron excitability indicates that C-boutons could be involved in modulating motor neuron excitability during ALS disease progression.

1.5 Hypothesis

The observation that a significant amount of denervation occurs in ALS patients and SOD1^{G93A} mice before the onset of motor symptoms suggests the existence of a compensatory mechanism that allows for the production of an equivalent motor output despite motor unit loss. The motor output of a muscle depends on the number and size of motor units recruited and the rate at which

they are firing (Winter, 1990). The progressive motor neuron death that occurs with ALS disease progression suggests that the compensatory mechanism likely involves modulation of motor unit firing rate rather than increased motor unit recruitment. Recently, cholinergic modulation of motor neurons through the C-boutons has been shown to increase motor neuron excitability (Miles et al., 2007) and changes in the C-bouton system have been observed in ALS patients and SOD1^{G93A} mice (Chang & Martin, 2009; Herron & Miles, 2012; Lasiene et al., 2016; Milan et al., 2015; Nagao et al., 1998; Pullen & Athanasiou, 2009; Saxena et al., 2013). Therefore, we hypothesized, "cholinergic modulation of motor neurons through the C-boutons increases the excitability of surviving motor neurons to compensate for motor unit loss during ALS disease progression." To test our hypothesis, we set out the following objectives:

1) Characterize the histological, physiological, and behavioural changes that occur throughout disease progression in high-expresser SOD1^{G93A} mice bred in our laboratory.
2) Determine whether $V0_C$ interneurons, which give rise to C-boutons, are active during locomotion in SOD1^{G93A} mice at ages of established denervation.
3) Determine whether silencing of the C-boutons in SOD1^{G93A} mice alters the characteristics of disease progression in SOD1^{G93A} mice.

Symptomatic treatments are the cornerstone of ALS patient care. An understanding of the mechanism that allows the body to innately compensate for motor unit loss can inform the development of therapies that specifically target the compensatory mechanism to potentially improve patient mobility and increase quality of life.

CHAPTER 2: MATERIALS AND METHODS

2.1 Animals

All experiments were done in accordance with the Canadian Council on Animal Care guidelines and were approved by the Dalhousie University Committee on Laboratory Animals. The $SOD1^{G93A}$ (B6.Cg-Tg(SOD1*G93A)) and wildtype (WT) mice used for this project were derived from a breeding pair obtained from the laboratory of Dr. Victor Rafuse at Dalhousie University. Mice were housed in the Life Science Research Institute Animal Care Facility on a 12-hour light/dark cycle (light from 07:00-19:00, dark from 19:00-7:00+1day) with *ad libitum* access to standard laboratory chow and water.

2.2 Construction of Electrode Set

2.2.1 Fabrication of Electromyogram Electrodes

Electromyogram (EMG) electrodes were created as previously described by Pearson et al (2005). EMG electrodes were made using seven-stranded, Teflon coated, annealed stainless steel wire (0.005 inches coated and 0.001 inches bare, A-M systems, Sequim, WA, Catalog Number 793200). Two strands of wire (approximately 13 cm in length) were tied together with a knot approximately 6 cm from one end to form a long end and a short end. Approximately 1 mm from the knot on the short end a 1 mm section of the Teflon insulation was removed from one of the paired wires. On the other wire, a 1 mm section of Teflon insulation was removed at a distance of 3 mm from the knot, creating two 1 mm sections of bare wire with a 1 mm separation. A 4 mm and a 1 mm section of insulation were removed from the short and long ends, respectively. The wires of the short end were twisted together and crimpled into the shaft of a 27-gauge needle. At

the other end, the 1 mm section of bare wire was soldered to a miniature connector (SamTech) (Pearson et al., 2005).

2.2.2 Fabrication of Nerve Stimulation Cuff Electrode

Nerve cuff electrodes were created as previously described by Akay (2014). A 1.5 mm section of AlliedSil Silicone Tubing (implant grade, P03; Allied Biomedical, Ventura, CA) was used to create the skeleton of the electrode. Two 9 cm wires (identical to those used for EMG electrodes) were bared 15 mm from one end, and 1 mm from the other end. Using a 32-gauge needle, the 15 mm bare ends of both wires were guided in parallel through the silicone tubing, creating a section of exposed wires on both sides of the tubing interior with small separations at the top and bottom of the tube. A suture (7-0, Perma-hand silk, Johnson&Johnson, Ontario, Canada) was guided between the two wires with approximately 2 cm of suture extending beyond the entry and exit sites at the top of the tube. A coating of Medical Silicone Adhesive (Dow Corning, Michigan, USA) was applied evenly to the entire exterior of the tube to ensure insulation of any exposed wire, and to maintain the parallel orientation of the wires. The silicone adhesive was left to cure overnight. The following day, the tubing was cut longitudinally between the entry and exit sites of the suture to open the tube.

2.2.3 Assembly and Construction of Cap

Three EMG recording electrodes and one nerve stimulation cuff were attached to a headpiece pin connector (female, SAM1153-12; DigiKey Electronics, Thief River Falls, MN) to form a complete set of electrodes as previously described (Pearson et al., 2005; Akay et al, 2006). The underside of the connector was coated with epoxy (Devcon 5 min Epoxy Gel, Massachusetts,

USA) to insulate the area of wire insertion (Pearson et al., 2005). Epoxy was used to extend the area of the connector to form a flat base referred to as the cap. Four holes (approximately 1 mm in diameter) were made in the cap (top, bottom, left, right) to serve as anchoring sites during implantation.

2.3 Implantation Surgery

All surgeries were performed aseptically on a water-circulated heating pad maintained at 42ºC. $SOD1^{G93A}$ and WT male mice were implanted with three EMG recording electrodes and one nerve stimulation cuff on the right side of the body at approximately P30-P70. Anesthesia was induced with isoflurane (5% for induction, 2% for maintenance). Once anesthetized, the right hind end and back of the neck were shaved and sterilized for surgery with a three-part skin scrub of hibitane, alcohol solution, and povidone-iodine. A small incision, large enough to accommodate the connector, was made in the skin of the dorsal neck region. An additional incision was made in the skin at approximately the hip joint. Saline lubricated tubing was inserted under the skin from the hip incision to the neck incision. The electrodes were fed through the interior of the tubing, leaving the cap in place at the opening of the neck incision and the electrodes exiting at the hip incision. The connector was sutured in place through the four holes in the cap using a 4-0 suture (Perma-hand silk).

Small incisions were made in the skin of the leg above each muscle to be implanted. The muscles implanted for these experiments were the tibialis anterior (TA), gastrocnemius (Gs), and the soleus (Sol) (Figure 1A). Implantation of the EMG electrodes was performed as previously

A EMG Recordings

TA:Tibialis Anterior
Sol:Soleus
Gs: Gastrocnemius

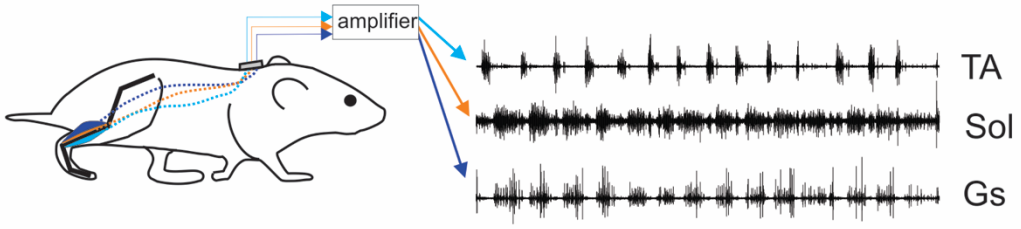

B Kinematics

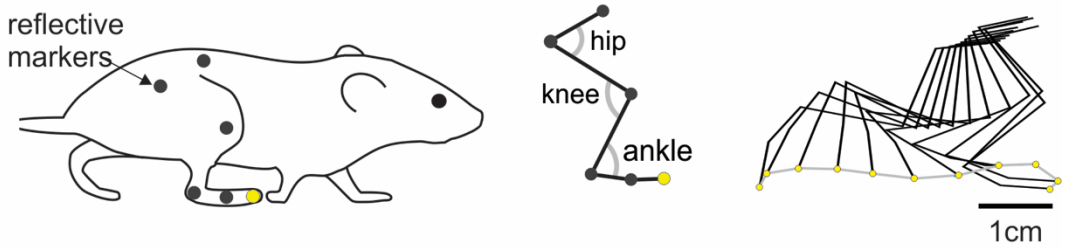

C Nerve Stimulation

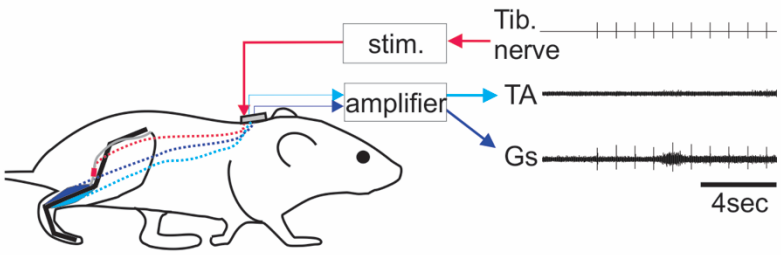

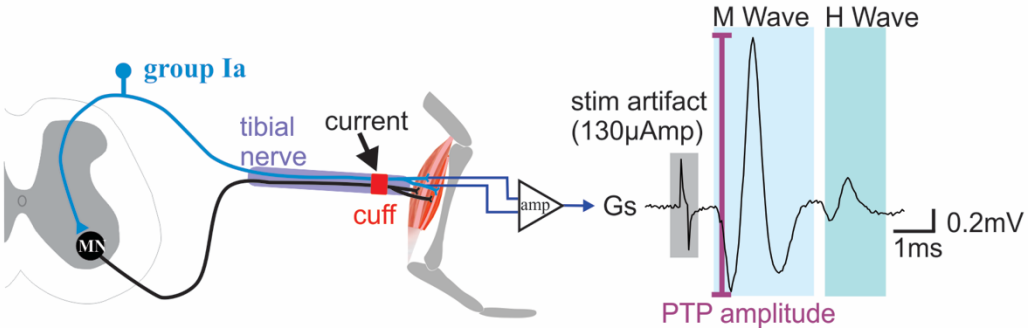

Figure 1. Methodology for monitoring disease progression in SOD1^{G93A} mice.
(A) EMG recording electrodes were implanted in the gastrocnemius (Gs), tibialis anterior (TA), and soleus (Sol) muscles and muscle activity was recorded during treadmill walking and swimming for SOD1^{G93A} and wild-type mice. **(B)** Kinematic data was obtained during treadmill walking and movement was reconstructed frame-by-frame by tracking reflective markers attached temporarily to the skin above the iliac crest, hip, knee, ankle, paw, and fourth digit. **(C)** The tibial nerve was stimulated with increasing currents (50μA – 1000 μA) while the EMG response was recorded in the Gs muscle. Stimulation of the tibial nerve causes an action potential in motor neurons that elicits a muscle response called the M-Wave. The peak-to-peak (PTP) amplitude of each M-Wave was measured and averaged for each stimulation strength. The largest average M-Wave is the Mmax or compound muscle action potential (CMAP). Changes in the CMAP were recorded from week to week in wild-type and SOD1^{G93A} mice. Stimulation of the tibial nerve also causes an action potential in Ia proprioceptive afferents that travels to the spinal cord and excites homonymous motor neurons through largely mono-synaptic connections, generating a second more delayed response at the muscle that is captured as the H-wave.

described (Pearson et al., 2005). Briefly, the needle at the end of the EMG electrodes was used to draw the wires through the muscle until the knot proximal to the bared regions was placed against the surface of the muscle. The distal end of the electrode exiting the muscle was tied into a knot against the surface of the muscle and the excess wire was cut off approximately 3mm from the knot.

As described previously (Akay, 2014), the tibial nerve was implanted by placing the nerve cuff adjacent to the nerve, and gently sliding the nerve into the interior of the cuff. The cuff was secured around the tibial nerve by forming a knot from the 7-0 sutures extending from the cuff. All incisions in the skin of the hind end were closed using 6-0 sutures (Perma-Hand silk). Mice were given buprenorphine (0.1 mg/kg) and ketoprofen (0.5 mg/kg) subcutaneously immediately after surgery, and subsequently every 12 hours (buprenorphine) and 24 hours (ketoprofen) for the following 48 hours. Mice were allowed to recover for 10 days before beginning any behavioural experiments.

2.4 Behavioural Experiments

2.4.1 Treadmill Kinematic and Electromyogram Recording

Once mice had fully recovered (approximately 10 days), recording sessions were performed weekly until $SOD1^{G93A}$ mice reached end-stage (~P150-P170), and WT mice reached an age equivalent to that of end-stage in $SOD1^{G93A}$ mice. Before each recording session, mice were briefly anesthetized using isoflurane to attach custom-made three-dimensional reflective markers (~2 mm diameter, cone shaped). Markers were placed at the level of the iliac crest, hip joint, ankle joint, paw joint, and the tip of the fourth digit using superglue (Lepage) to adhere them in place

(Figure 1B). As the skin superficial to the knee joint is loose, the knee position is triangulated using the length of the femur and tibia (measured each week) rather than a reflective marker to improve accuracy. Mice were removed from anesthesia and placed on a 25x6x16 cm (length x width x height) treadmill (Model 802; Zoological Institute, University of Cologne, Cologne, Germany) and connected to the amplifier (Model 102; Zoological Institute, University of Cologne, Cologne, Germany).

Prior to each recording, a short video (approximately 10 ms) is taken of the calibration block, which has four reflective markers forming a 7 cm x 4 cm rectangle. The calibration video is later used for transformation of kinematic data. After full recovery from anesthesia (approximately 5 minutes) mice began walking on the treadmill at a speed of 0.2 m/s. Videos capturing the locomotion of the mice were taken from the right side using a high-speed camera at 250 frames per second (Fastec IL3-100, San Diego, CA, USA) and a spotlight to illuminate the markers. Muscle activity was simultaneously recorded via EMG electrodes (sampling rate of 10 kHz) using Power1401 interface and Spike2 software (Cambridge Electronic Design, Cambridge, United Kingdom). After two high-speed videos of mice walking at 0.2 m/s were recorded (containing consistent walking), the maximal walking speed of each mouse was tested. EMG activity from the Gs, TA, and Sol muscles was sampled throughout the entire walking experiment (Figure 1A) to be later synchronized with videos containing kinematic data. Mice walked at increasing speed increments of 0.1 m/s until they could no longer keep up with the treadmill. A mouse was considered capable of a certain speed if they could take a minimum of 8 steps without lagging to the back of the treadmill.

2.4.2 Nerve Stimulation

After completion of walking behaviour experiments, the tibial nerve was stimulated with 2 ms pulses at a 1 Hz frequency with gradually increasing stimulation strengths (Figure 1C). The EMG responses at the Gs (sampling rate of 25kHz) and Sol (sampling rate of 10kHz) muscles were recorded for each stimulation in resting animals. A Biphasic Stimulus Isolator (DS4; Digitimer, Hertfordshire, United Kingdom) controlled by Spike2 and Power 1401 were used to deliver the electric currents. The direction of current flow through the nerve cuff was held constant from week to week in all animals.

2.4.3 Electromyogram Recording during Swimming

To compare muscle activity during different forms of locomotion, EMG activity (sampling rate of 10 kHz) was recorded during swimming in a 30x3x7 inch (length x width x height) rectangular custom-made swimming pool. Water temperature was approximately 28°C. Time periods where the mouse was actively swimming (versus treading water) were marked and only these sections were used for data analysis.

2.5 Analysis of Behavioural Experiment Data

2.5.1 Digitizing Markers from Treadmill Videos

Marker locations during treadmill locomotion were digitized using two different programs. Vicon Motus Motion Analysis software (Vicon, Centennial, CO) was used for approximately two-thirds of the experiments. First, the raw coordinates of the four markers on the calibration block are identified. Then, for each marker on the mouse, the predictor radius (restricted region the marker could appear within in the next frame) and maximum and minimum marker sizes were

inputted into the software which automatically tracked marker positions throughout. The software then converts the raw coordinates of the joint markers into scaled coordinates, triangulates the knee position (using scaled coordinates and the length of the femur and tibia), and calculates angular movement about the hip, knee, ankle, and paw joints.

The remainder of kinematic experiments were analyzed using scripts for Image J (Kinema J) and R (Kinema R) written by Dr. Nicolas Stifani. Using Kinema J, a rectangular box was drawn to connect the four calibration markers on the calibration block, and used to determine the conversion coefficient for converting pixels to centimeters. Next, the intensity threshold of the treadmill videos was adjusted to illuminate only the reflective markers. The X and Y coordinates of each marker (in pixels) were tracked frame by frame for the entire video. The output of Kinema J, the marker coordinates in pixels, were then transformed into centimeter values using the conversion coefficient calculated from the calibration videos by Kinema R. Kinema R triangulated the knee position (using the transformed coordinates of the hip and ankle joint and the length of the femur and tibia) and calculated the joint angles.

2.5.2 Analysis of Kinematic Data

Kinematic parameters were imported into Spike2 files containing the corresponding EMG data using a custom Spike2 script that precisely synchronizes the two types of data. The onset and offset of swing phase were identified using the slope of the toe x-axis position. Slope values rising through zero marked the onset of swing phase, and slope values falling through zero marked the offset of swing phase. A custom-made Spike2 script was used to calculate the step duration (time elapsed from the beginning of stance phase to the end of swing phase), swing phase duration (time

elapsed from beginning to end of swing phase), stance phase duration (time elapsed from beginning to end of stance phase), and swing amplitude (toe x position at swing onset subtracted from toe x position at swing offset). The output of the script was the step duration, swing duration, stance duration, and swing amplitude for each step in a span of 10-30 steps. This data was copied into Microsoft Excel 2016 and the average and standard deviation was calculated for each of the four parameters.

The average angular joint movements for the hip, knee, and ankle joints were calculated using the "Waveform Average" analysis function in Spike 2 for 10-30 steps. Analysis of joint angles for each step was triggered by the swing offset and were measured for 0.9 seconds (0.3 seconds before swing offset, 0.6 seconds after swing offset). The average angular joint movements for each joint were exported to Microsoft Excel 2016 where the maximum and minimum possible angles were determined. The average range of motion (ROM) for the hip, knee, and ankle joints was determined by subtracting the minimum joint angle value from the maximum (ROM= maximum angle – minimum angle).

2.5.3 Analysis of Electromyogram Data

To determine the amplitude of the muscle activity burst during locomotion, the EMG data from walking and swimming behaviours were analyzed using the same method. An event channel was created in the Spike2 EMG files, and the beginning of each burst was marked for a single muscle (typically the TA) during a period of consistent locomotion. Approximately 30-60 bursts were analyzed per mouse, per week. The Gs, Sol, and TA channels of the recording were rectified, smoothed (0.005 time constant), and the DC offsets were removed prior to analysis. A custom-

made Spike2 script was used to identify the maximum and minimum values for each burst in each muscle and then calculate the respective amplitudes. The bursting amplitude for each muscle was then averaged using Microsoft Excel 2016.

To compare differences in muscle activation during walking and swimming, a ratio of the amplitude of muscle activation during swimming compared to walking was calculated (ratio = amplitude during swimming ÷ amplitude during walking) for each muscle.

2.5.4 Analysis of Nerve Stimulation Data

Each week, the compound muscle action potential (CMAP) was recorded and changes in CMAP throughout lifespan were assessed. The CMAP was calculated by analyzing the average Gs response during each current increment to determine the time delay from the current impulse to the beginning of M wave and to the end of M Wave (Figure 1C). The M wave onset and offset values that best describe the M wave delay for all stimulation strengths was used. A custom-made Spike 2 script calculates the peak-to-peak amplitude of the Gs activity after each current impulse in the delay range specified. The data was exported to Microsoft Excel 2016 and the average M wave response and standard deviation for each current step was calculated. The current step with the highest average M wave response is the CMAP. The CMAP from each recording was graphed for each mouse and normalized to the maximum value recorded during the experiment. The same measurements were performed to analyze H wave, however, the data was not fully analyzed because the small size of the mouse causes the H wave to be contaminated by the M wave, thereby producing imprecise data.

2.6 Generation of ALS Mice with Silenced C-Boutons

To investigate whether C-boutons are involved in behavioural compensation in ALS, we generated a SOD1^{G93A} mouse with silenced C-boutons (*SOD1^{G93A} ; Dbx1::Cre ; ChAT$^{flox/flox}$*), herein referred to as SOD1;C^{OFF}. The neuronal source of C-boutons are V0$_C$ interneurons which are derived from small cluster of Pitx2+ V0 (Dbx1+) interneurons that form a longitudinal column near the central canal (Zagoraiou et al., 2009). The *Dbx1::Cre* mice used to generate this cross were obtained from the laboratory of Dr. Robert Brownstone at Dalhousie University. *ChAT^{flox}* mice (*Chat^{tm1Jrs}*) were obtained from Jackson Laboratory and bred in house for homozygosity before further crossing.

2.7 Histology

All mice were anesthetized with Euthanyl (100µl sodium pentobarbital, 100 mg/kg, intraperitoneal, Bimeda-MTC, Ontario, Canada) and transcardially perfused with cold phosphate buffered saline (PBS, 20ml) and 4% paraformaldehyde (PFA, 10ml). The Gs, Sol, and TA muscles were immediately dissected and weighed before being cryoprotected in 30% sucrose for 24 hours. Spinal cords were dissected and post-fixed in 4% PFA for 24 hours prior to cryoprotection in 30% sucrose for 48 hours. The spinal cord was then segmented into L2, L3-4, and L5. All tissue was frozen in Optimum Cutting Temperature compound (Tissue-Tek, Sakura Finetek, USA) and stored in the -80ºC freezer. Muscle tissue was serially sectioned at 40µm using a cryostat and placed onto slides (20 slides for Gs, 8 slides for TA, and 6 slides for Sol) such that each slide was a representation of the whole muscle. Spinal cords were sectioned serially at 30µm using a cryostat and placed onto slides (6 slides for L2, 12 slides for L3-4, and 6 slides for L5). Slides were dried overnight at room temperature and placed in the -80ºC freezer for long term storage. Prior to

immunohistochemistry, slides were removed from the -80ºC freezer and left at room temperature for one hour. Sections were washed 3 x 10 minutes with 1X PBS/0.3% Triton X-100 (0.3% PBST) before blocking with 4% bovine serum albumin (BSA)/0.3% PBST for one hour.

2.7.1 Neuromuscular Junction Analysis

For NMJ analysis, the co-localization of the pre-synaptic motor neuron and the muscle fiber motor end plate was assessed. To label the pre-synaptic motor neuron, the primary goat anti-VAChT antibody (ABN 100, Millipore) was used (1:1000 dilution with 1%BSA/0.3% PBST). To label the motor end plate, tetramethylrhodamine α-bungarotoxin (T1175, Life Technologies, California) which binds to nicotinic acetylcholine receptors, was used (1:200 dilution with 1%BSA/0.3% PBST). Primary antibodies were incubated overnight at 4ºC in a humidified chamber. The following day, sections were washed 3 x 10 minutes in 0.3%PBST, and incubated with a donkey anti-goat 488 (1:1000, Life Technologies, California) secondary antibody at room temperature for 2.5 hours, followed by 3 x 10 minute washes with PBS.

NMJs were counted using a Leica BM LB2 fluorescent microscope. The extent to which the pre-synaptic motor neuron (VAChT, green) and the post-synaptic motor end plate (BTX, red) were co-localized was assessed. Each NMJ was classified as innervated, partially innervated, or denervated. A motor end plate was considered to be innervated if there was complete co-localization of the BTX and VAChT labelling. Partially innervated was assigned when the motor terminal labelling (VAChT) was partially, but not completely co-localized with the motor end plate. Finally, motor end plates were counted as denervated if only a BTX labelled motor end plate

was observed with no VAChT co-localization. All sections on one slide were manually counted for each animal.

2.7.2 Neuronal Activation Using c-fos

To determine whether C-boutons are involved in compensation, we assessed the activation of $V0_c$ neurons during walking and swimming at disease stages identified as symptomatic in $SOD1^{G93A}$ mice, and the equivalent ages in WT mice. The symptomatic age range of P>100 was chosen based on the previous reports of symptom onset (Chiu et al., 1995; Gurney et al., 1994) and the observation that at P100 innervation of the Gs and TA is below 50%. For the resting condition, mice were removed from their home cage and perfused immediately. In the walking condition, mice walked on the treadmill for one hour divided into intervals consisting of four minutes of walking and one minute of rest for a total of 12 intervals. All WT mice walked at 0.2m/s for the entire hour. $SOD1^{G93A}$ mice all started the experiment walking at 0.2m/s, but the speed had to be reduced over the course of the hour due to fatigue. In this case, the speed was set to the maximum speed at which the $SOD1^{G93A}$ mice could complete the four-minute interval. For the swimming condition, WT mice swam for a total time of 40 minutes with short (~30-60 second) breaks where mice were removed from the pool when they would no longer swim. Mice readily began swimming again when placed back in the pool. There were no $SOD1^{G93A}$ mice in the swimming condition.

All animals were perfused one hour after completion of the locomotor task and spinal cord tissue was processed as outlined above. The L3-4 sections of the spinal cord were used for analysis based on previous reports that cholinergic Pitx2+ interneurons, the sole source of the C-boutons,

are predominantly located in upper lumber regions of the spinal cord (Zagoraiou et al., 2009). The primary rabbit anti-c-fos antibody (1:10000 dilution with 1%BSA/0.3%PBST, Cedarlane 226003) was used as a marker of neuronal activation and goat anti-ChAT (1:250 dilution with 1%BSA/0.3%PBST, AB144P, Millipore) was used as a marker of cholinergic neurons. Primary antibodies were incubated overnight at 4ºC in a humidified chamber. The following day, sections were washed 3 x 10 minutes in 0.3%PBST, and incubated with donkey anti-goat 488 (1:1000, Invitrogen, Carlsbad, CA) and donkey anti-rabbit 555 (1:1000, AB150075) secondary antibodies at room temperature for 2.5 hours, followed by 3 x 10 minute washes with PBS.

C-fos expression in the $V0_C$ interneurons was viewed using the Leica BM LB2 fluorescent microscope and qualitatively assessed. $V0_C$ interneurons were identified based on their expression of ChAT and location in the vicinity of the central canal in lamina X.

2.8 Statistics

Statistical analysis was performed on range of motion and gait parameter data using Graph Pad Prism 6.07 software (GraphPad Software, San Diego, CA). Comparisons between the P40-59 age range and the P60-79, P80-99, P100-119, P120-139, and P>140 were made within the same genotype only (i.e., $SOD1^{G93A}$ mice were only compared with younger $SOD1^{G93A}$ mice). No comparisons were made between genotypes or between ages other than those listed above. All statistics were calculated using two tailed-unpaired Student's t-tests when normality was achieved. If normality was not achieved, Mann-Whitney tests were used to compare between the two groups. Statistical significance was considered to be achieved if $p< 0.05$.

CHAPTER 3: RESULTS

3.1 Effect of Muscle Fiber Type on Muscle Denervation

The extent of muscle denervation is an important indicator of disease progression in animal models of ALS. As disease progression is highly variable between animal models of ALS and between laboratories using the same model (Kanning et al., 2010), the onset and rate of muscle denervation was characterized in our high-expresser SOD^{G93A} mouse line. Previous studies have shown that large, fast motor units are more susceptible to denervation than small, slow motor units (Atkin et al., 2005; Frey et al., 2000; Hegedus et al., 2007). Therefore, we examined neuromuscular junction innervation and muscle wet weights throughout disease progression to determine the extent of denervation and muscle atrophy, respectively. Two fast-twitch muscles, the tibialis anterior (TA) and gastrocnemius (Gs), and one slow-twitch muscle, the soleus (Sol) were analyzed using histology. The Gs was also analyzed indirectly through stimulation of the tibial nerve and a recording EMG electrode in the Gs muscle.

3.1.1. Histological Analysis of NMJ Innervation and Muscle Wet Weight

Neuromuscular junction innervation (Figure 2A) was assessed in Gs, TA, and Sol muscles from WT and $SOD1^{G93A}$ mice. NMJs were classified as innervated, partially innervated, or denervated based on the degree of overlap between the VAChT-positive motor axon terminals and the BTX-labelled motor end plates. Innervation of the Gs muscle was above 85% in WT mice at all ages analyzed (Figure 2B). In contrast, innervation of the Gs muscle in $SOD1^{G93A}$ mice dropped suddenly from 95% at P55 to 34% at P61. Following this large initial drop, Gs innervation recovered slightly and was relatively constant at ~50% from P70-P110. Notably, there are three

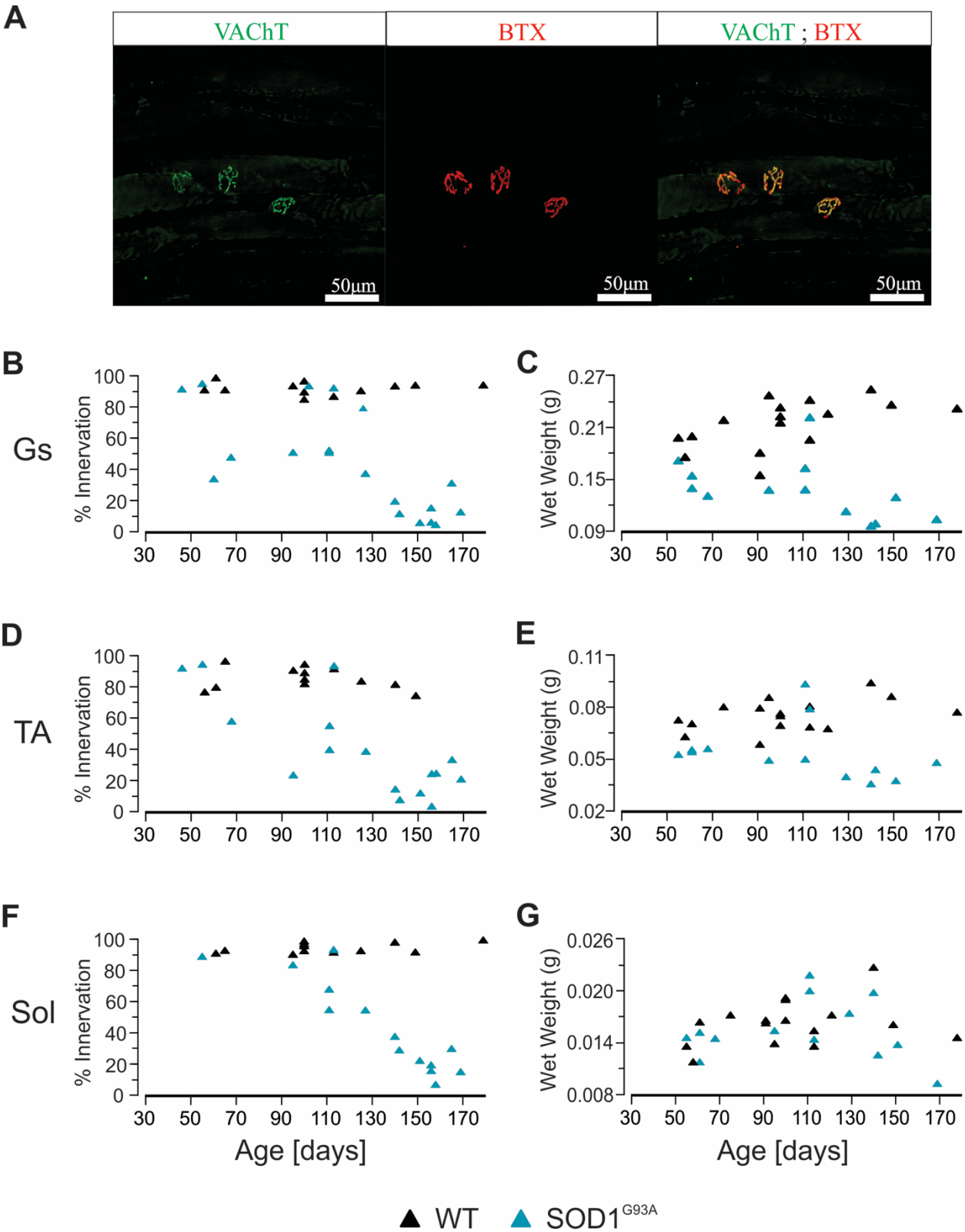
A
VAChT
BTX
VAChT ; BTX
50µm
50µm
50µm
B
Gs
% Innervation
C
Wet Weight (g)
D
TA
% Innervation
E
Wet Weight (g)
F
Sol
% Innervation
G
Wet Weight (g)
Age [days]
Age [days]
WT
SOD1G93A

Figure 2. Neuromuscular junction innervation and muscle wet weight in WT and SOD1^{G93A} mice.

Neuromuscular junction innervation was assessed based on the degree of overlap between VAChT (green) positive motor axon terminals and BTX (red) labelled motor end plates **(A)**. The percentage of innervation was calculated for the gastrocnemius (Gs) **(B)**, tibialis anterior (TA) **(D)**, and soleus (Sol) **(F)** muscles in wild-type and SOD1^{G93A} mice. The muscle wet weight, an indicator of muscle atrophy, was also recorded for the Gs **(C)**, TA **(E)**, and Sol **(G)**. Note the early denervation of the Gs and TA muscles at ~P60 and ~P70, respectively, and the later denervation of the Sol muscle at ~P110.

data points from P100-P125 where innervation of the Gs is >80% in SOD1^{G93A} mice. After P125, Gs innervation dropped below 40% and continued to decline with some variability as the disease progressed. At P169, the oldest age of the SOD1^{G93A} mice examined, Gs innervation was 13% (Figure 2B). The wet weight of the Gs muscle is lower in SOD1^{G93A} mice than in WT mice at nearly all ages (one exception, P113) and began to decline in SOD1^{G93A} mice at ~P120 as the muscle began to atrophy (Figure 2C).

Innervation of the TA muscle was ≥75% in WT mice at all ages analyzed (Figure 2D). In SOD1^{G93A} mice, TA innervation dropped from 95% at P55 to 59% at P68. Between P70 and P130, innervation was highly variable, but tended to be around 40-60%. At P169, TA innervation was 21% in SOD1^{G93A} mice (Figure 2D). The wet weight of SOD1^{G93A} TA muscles was consistently lower than WT mice (with two exceptions: P111, P113), but there were overall no drastic changes in wet weight throughout disease progression in SOD1^{G93A} mice (Figure 2E).

Innervation of the Sol muscle was above 90% at all ages of WT mice examined (Figure 2F). In contrast, the Sol innervation in SOD1^{G93A} mice began to slowly decline from ~90% at P55 to less than 20% by ~P155. Notably, the progression of denervation of the Sol muscle occurs gradually, whereas the denervation of the Gs and TA muscles occurs in large drops (Figure 2F). The wet weights of the WT and SOD1^{G93A} Sol muscles are similar throughout life until ~P150 when the disease is quite progressed and SOD1^{G93A} Sol wet weights begin to fall below WT (Figure 2G).

3.1.2 Electrophysiological Analysis of Muscle Innervation

To provide a continuous *in vivo* measurement of Gs muscle innervation, the CMAP in response to stimulation of the tibial nerve was measured each week in WT and SOD1^{G93A} mice for the duration of the experiment. The CMAP, expressed as a percentage of the maximum value, tended to increase with age in WT mice from the beginning of the experiment (~P45) to the end (~P170) (Figure 3A-C). In one case, the CMAP began to decrease at P104 (Figure 3A) and we were unable to determine whether it would recover because the animal was euthanized due to removal of the electrode cap. The trend of the CMAP to increase with age in WT mice can be further observed in Figure 3D which shows the CMAP of all mice recorded in the experiment. The CMAP of SOD1^{G93A} mice increased during the first few weeks of the experiment (~P45-P90) before dropping abruptly to ~50% of the maximum at ~P100 (Figure 3E-G). Following the large drop, the CMAP tended to slowly decline until end stage of the disease with the exception of one animal (Figure 3G) in which the CMAP began to increase again at P134. In the other two animals, CMAP is ~15% at end-stage (Figure 3E, F). Figure 4H provides an overall picture of the CMAP changes observed in all SOD1^{G93A} mice recorded during the experiment. Overall, Gs CMAP data indicates that a large portion of Gs motor units are lost by P115 in SOD1^{G93A} mice.

3.2 Minimal Motor Phenotype Despite Established Motor Unit Loss

Although CMAP data indicates that SOD1^{G93A} mice lose the function of a large portion of their motor units beginning at ~P100, locomotor behaviour does not markedly change until ~P130-140 when the pelvis starts to drop and the mice begin to lose the ability to walk at faster speeds (0.4-0.5m/s). Prior to this, the first detectable visual change in locomotion in SOD1^{G93A}

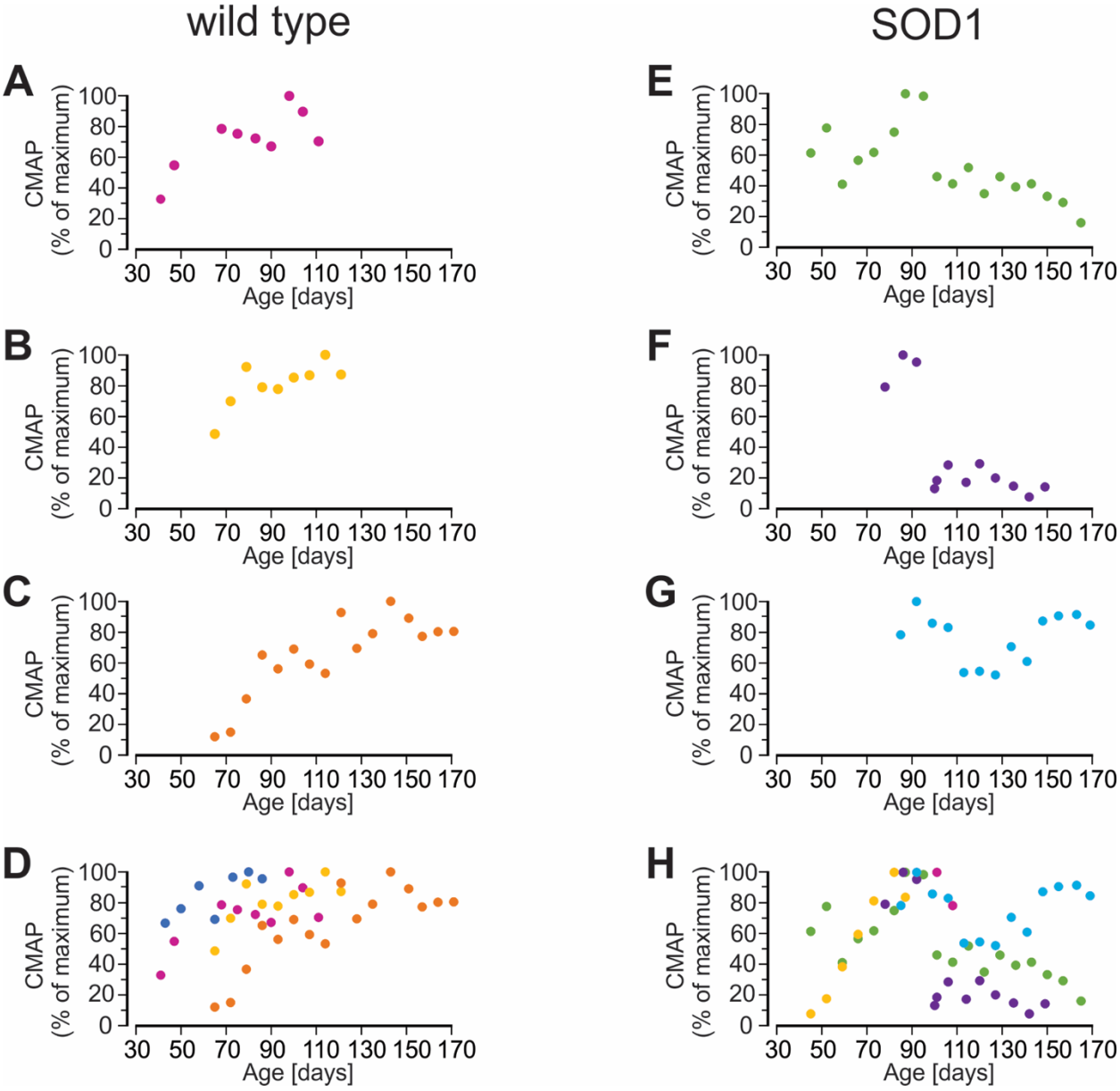

Figure 3. Large Changes in CMAP occur in SOD1^{G93A} Mice at ~P100.
Changes in the compound muscle action potential (CMAP) were used to measure changes in muscle innervation in individual wild-type and SOD1^{G93A} mice across time. CMAP measurements representative of wild-type **(A-C)** and SOD1^{G93A} **(E-G)** mice are shown individually for clarity. Note the large drop in CMAP to ~50% of maximum in all SOD1^{G93A} mice at ~P90. Graphs of CMAP recordings from all wild-type and SOD1^{G93A} mice are shown in **D** and **H**, respectively. Each individual animal was assigned a different coloured dot. All CMAP values are expressed as a percentage of the maximum CMAP value measured during the experiment for each animal.

mice occurred at ~P84 (83.87days ±3.18 days) when a very subtle abnormality in the movement of the ankle joint throughout swing phase was observed. While the change in ankle movement could only be observed in videos when they were slowed down to half-speed, this difference was readily detectable in the EMG and kinematic data. In WT mice, as the leg moved through swing phase, the angles about the hip, knee, and ankle joints displayed smooth, continuous motion accompanied by large singular bursts of EMG activity in the Gs and TA (Figure 4A, C). In contrast, at ~P84 in SOD1^{G93A} mice, the movement of the leg through swing phase became more disjointed and the TA activity profiles changed from a singular large burst to multiple small bursts. These small, frequent bursts of TA activity coincided with small fluctuations in the angular movement of the ankle joint (Figure 4B, D). As the disease continued to progress, the bursts of TA activity became increasingly smaller and more numerous (Figure 4B, P129). As this remained the only visually detectable symptom of muscle weakness during walking until ~P130, we investigated whether any locomotor changes could be seen in SOD1^{G93A} mice during swimming.

3.3 Task Dependent Upregulation of Gs Activity is Impaired with ALS Disease Progression

To determine whether ALS disease progression differentially affects locomotor behaviour during swimming compared to walking, EMG activity was recorded during swimming and compared to that obtained during walking.

In WT mice, the amplitude of the Gs muscle burst during swimming was consistently larger than the burst observed during treadmill walking at 0.2m/s (Figure 5A). An increase in the Gs amplitude can be attributed to either the recruitment of additional motor units or an increase in the

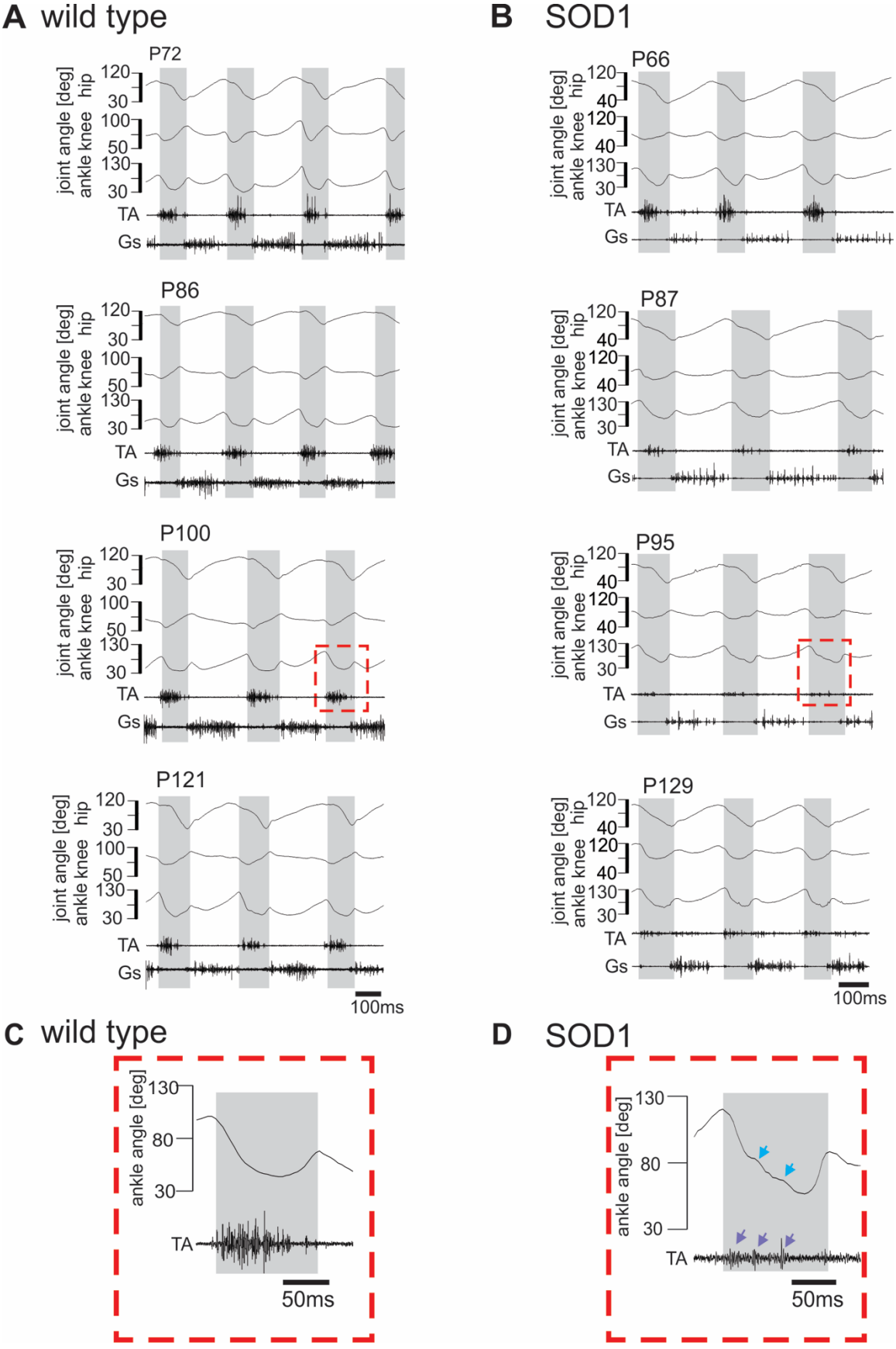
A wild type
B SOD1
P72
P66
P86
P87
P100
P95
P121
P129
joint angle [deg]
hip
knee
ankle
120
30
100
50
130
40
TA
Gs
100ms
C wild type
D SOD1
ankle angle [deg]
130
80
30
TA
50ms

Figure 4. Changes in the TA activity profile and ankle angle occur in walking SOD1^{G93A} mice at ~P84.

EMG activity of the TA and Gs muscles and angular movement of the hip, knee, and ankle joints during 0.2 m/s treadmill walking is shown at various ages in a wild-type mouse **(A)** and a SOD1^{G93A} mouse **(B)**. In wild-type mice, the swing phase is characterized by smooth changes in angular movement of the ankle and large, singular bursts of TA muscle activity **(A**, enlarged in **C)**. In SOD1^{G93A} mice, the TA activity profile during swing phase switches from a large, singular burst to multiple small bursts at ~P84. Bursts of TA muscle activity coincide with small fluctuations in the ankle joint **(B,** enlarged in **D)**.

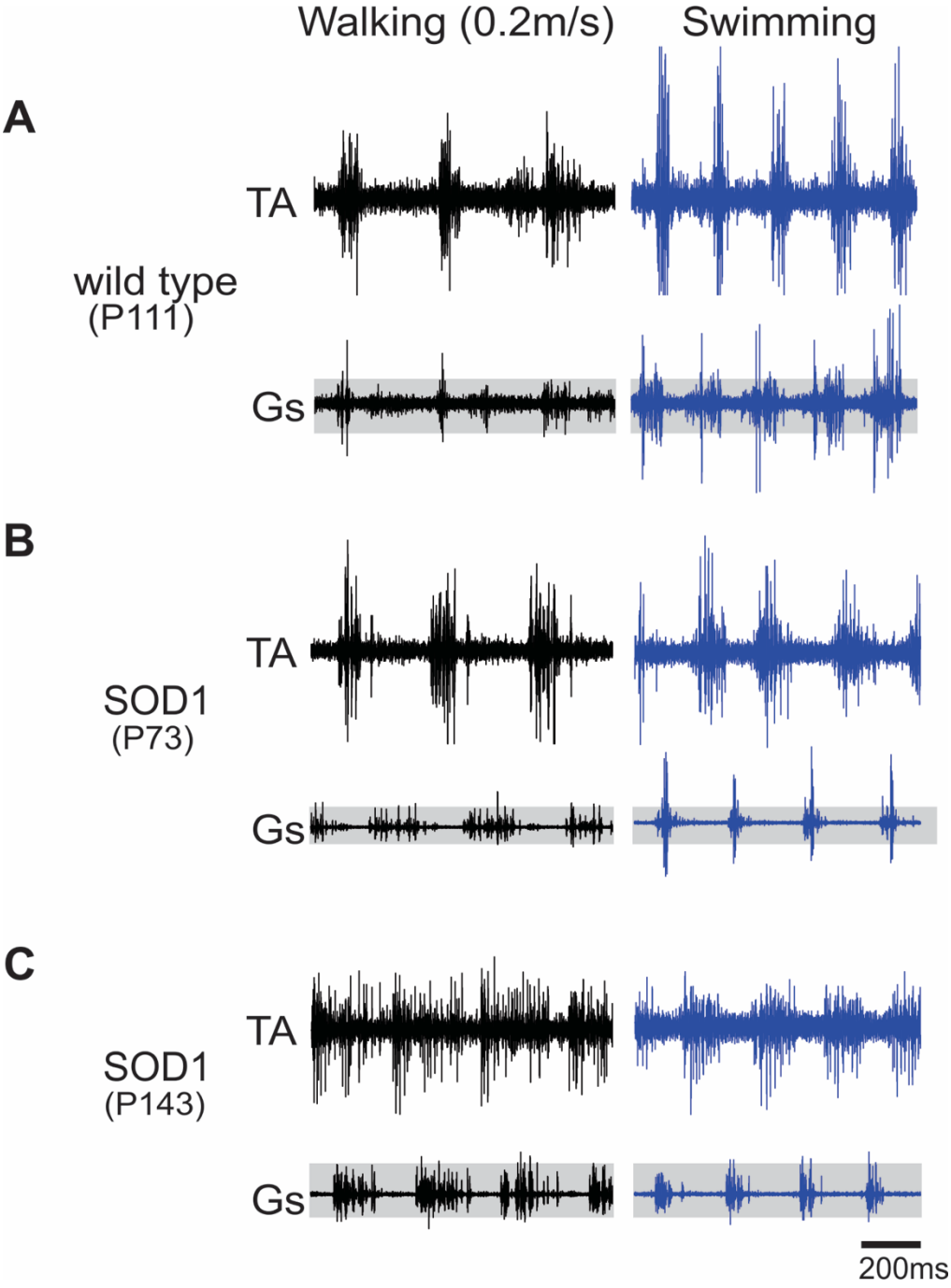

Figure 5. Deficits in task-dependent upregulation of Gs activity at later ages in SOD1^{G93A} mice.
EMG recordings of TA and Gs muscle activity during walking at 0.2m/s and swimming in a wild-type mouse **(A)** and a SOD1^{G93A} mouse at P73 **(B)** and P143 **(C)**. Grey bars in the background of Gs EMG recordings approximate the amplitude of Gs muscle activity during walking. Note the absence of Gs activity upregulation during swimming in the SOD1^{G93A} mouse at P143 (C).

firing rate of motor units already active. The increased Gs amplitude during swimming compared to walking was also observed in SOD1^{G93A} mice at ages prior to the drop in CMAP (before ~P100) (Figure 5B). However, as SOD1^{G93A} mice aged and lost the functionality of an increasing number of motor units, the ability to upregulate Gs activity during swimming was impaired and similar amplitudes of Gs activation were observed during walking and swimming (Figure 5C).

Changes in muscle activity during walking and swimming were quantified by calculating the swimming:walking ratio of Gs EMG activity and monitoring changes in this ratio over time. In WT mice, the ratio fluctuated from week to week, yet there was an overall upward trend and all ratios were above 2 at the time of the final recording (Figure 6A). In SOD1^{G93A} mice, the Gs swimming:walking ratio dropped below 2 at ~P90 and remained at values between 0 and 2 in the majority of mice for the remainder of the experiment (until animals could no longer swim) (Figure 6B). Data from all experimental WT and SOD1^{G93A} mice are shown in figure 6C and 6D, respectively. In general, the swimming:walking Gs activity ratio is rarely below 2 after ~P90 (Figure 6C), whereas in all SOD1^{G93A} mice examined the Gs activity ration is rarely above 2 after ~P90 (Figure 6D).

In summary, by ~P90 SOD1^{G93A} mice can no longer upregulate Gs activity during swimming (Figure 6D) and the CMAP has dropped to ~50% of the maximum value by ~P100 (Figure 3H). At this time, the only locomotor change observed was spasticity in the TA muscle during swing phase that caused fluctuations in the ankle angle (Figure 4B, D). Based on these

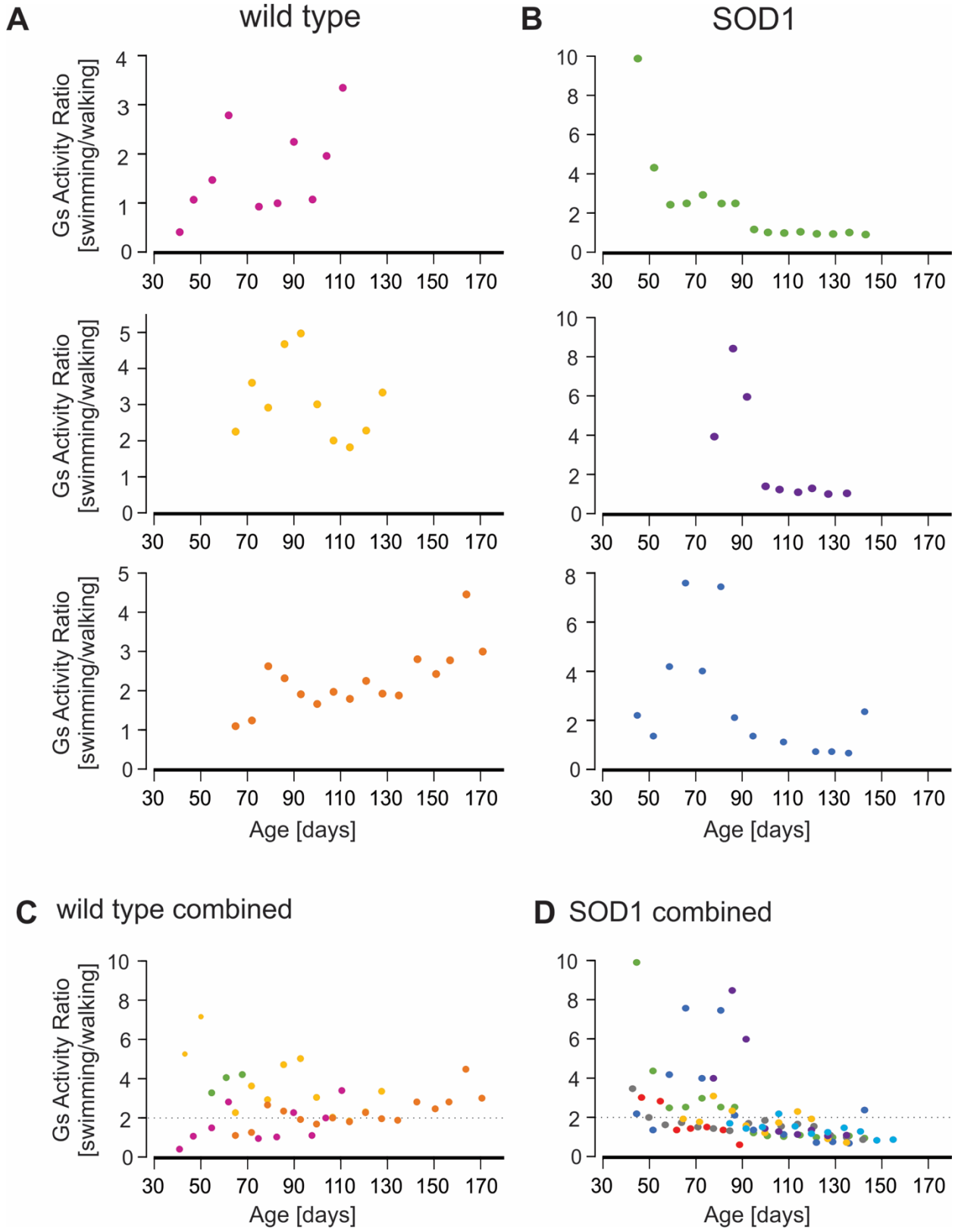
A
wild type
B
SOD1
Gs Activity Ratio [swimming/walking]
Age [days]
C
wild type combined
D
SOD1 combined

Figure 6. Changes in the swimming:walking ratio of Gs activity with age in SOD1^{G93A} mice. Ratios of the Gs EMG amplitude during walking and swimming were calculated across time for individual wild-type **(A)** and SOD1^{G93A} **(B)** mice. Note the large drop in the ratio at ~P90 in SOD1^{G93A} mice (B). Ratio data collected from all animals is displayed in **C** for wild-type mice and **D** for SOD1^{G93A} mice. Each different coloured dot represents data from a different animal. The dotted line crossing the y-axis at a Gs activity swimming:walking ratio of 2 shows that beyond ~P90 few wild-type mice have a Gs activity ratio below 2 (C), whereas few SOD1^{G93A} mice have a Gs activity ratio above 2 (D).

observations, we concluded that a compensatory mechanism must exist to modulate the activity of surviving motor neurons, thereby producing a phenotypically negative locomotor pattern in SOD1^{G93A} mice despite the known loss of functional motor units.

3.4 Hypothesis: C-Boutons Help Compensate for Motor Neuron Loss in SOD1^{G93A} Mice

The ability of SOD1^{G93A} mice to produce normal locomotor behaviour (Figure 4B, D) despite established motor unit loss (Figure 2B, D, F and Figure 3E-H) indicates either an increase in motor unit recruitment or an increase in excitability of remaining motor units. As motor neurons are degenerating during ALS disease progression, a modification of motor unit excitability is more likely to represent a potential compensatory mechanism.

C-boutons have previously been shown to increase motor neuron excitability (Miles et al., 2007) and to modulate Gs activity to match the biomechanical demands of different locomotor tasks (Zagoraiou et al., 2009). Therefore, we hypothesized, "cholinergic modulation of motor neurons through the C-boutons increases the excitability of surviving motor neurons to compensate for motor unit loss during ALS disease progression." In WT mice, C-boutons increase the excitability of motor units during swimming by increasing their firing frequency and therefore producing a greater contraction of the Gs muscle than that produced during walking (Figure 7A-B). Based on our hypothesis, we expect that when SOD1^{G93A} mice begin to lose motor units, the V0$_C$ interneurons giving rise to C-boutons will become active during walking. C-bouton activity will increase the excitability of the surviving motor units during walking and therefore facilitate the production of a muscular contraction equivalent to a WT mouse or a SOD1^{G93A} mouse prior to motor unit loss (Figure 7C). Furthermore, based on the decline of the Gs swimming:walking

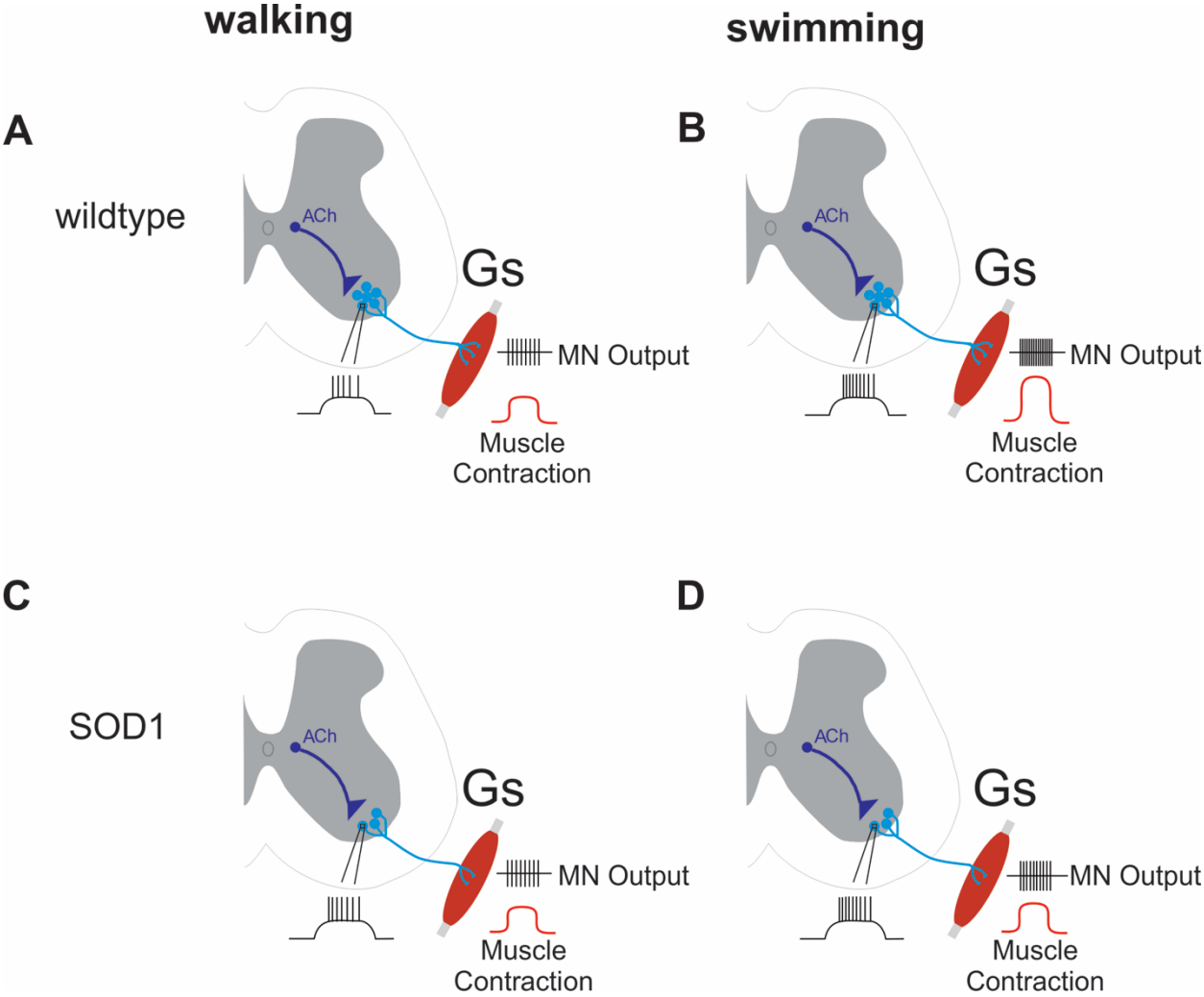

Figure 7. Cholinergic modulation of motor neurons through C-boutons underlies compensation for motor unit loss in SOD1^{G93A} mice.
(A) V0$_C$ interneurons (dark blue) are relatively inactive during walking in wild-type mice and do not influence motor output or muscle contraction. **(B)** V0$_C$ interneurons are active during swimming in wild-type mice and release acetylcholine (ACh) through the C-boutons to increase motor neuron excitability. Increased motor neuron excitability increases the motor output and produces a larger contraction of the Gs muscle. **(C)** When motor neuron death occurs in SOD1^{G93A} mice, cholinergic modulation through the C-boutons increases the excitability of the surviving motor neurons to generate motor output and Gs muscle contractions of the same magnitude as wild-type mice. **(D)** When SOD1^{G93A} mice are swimming, V0$_C$ interneurons are active and increase motor neuron excitability through the C-boutons. The increased motor neuron excitability produces a larger motor output and Gs muscle contraction than during walking in SOD1^{G93A} mice. However, as motor neuron excitability is already increased for walking in SOD1^{G93A} mice, the extra boost provided during swimming is insufficient to produce motor output and Gs muscle contractions of the same magnitude as wild-type mice during swimming.

activity ratio in SOD1^{G93A} mice after ~P90, we proposed that C-boutons are unable to provide as large of an excitability boost to Gs motor neurons during swimming because there is a limit to how quickly motor neurons can fire and they are already being excited
by the C-boutons during walking. As a result, there is a smaller contraction of the Gs muscle of SOD1^{G93A} mice during swimming than in WT mice or early stage SOD1^{G93A} mice (Figure 7D).

To test the hypothesis, "cholinergic modulation of motor neurons through the C-boutons increases the excitability of surviving motor neurons to compensate for motor unit loss during ALS disease progression," we investigated the following research questions:

1) Do SOD1^{G93A} mice lose the ability to upregulate Gs activity during swimming with ALS disease progression? (shown in Figure 6 B,D)

2) Do V0$_C$ interneurons (neuronal source of C-boutons) become active in SOD1^{G93A} mice with ALS disease progression?

3) Do SOD1^{G93A} mice with silenced C-bouton activity display an altered behavioural phenotype or lack of compensation during walking?

3.5 Activation of V0$_C$ Interneurons During Walking in SOD1^{G93A} Mice with Disease Progression

Using c-fos immunohistochemistry, we qualitatively assessed the activation of V0$_C$ interneurons in WT and SOD1^{G93A} mice at P>100 under resting and walking conditions and in WT mice during swimming. There are no specific immunohistochemical markers for V0$_C$ interneurons, rather they are identified based on ChAT expression and location in the vicinity of the central canal in lamina X. Under resting conditions at all ages no activity was observed in the putative V0$_C$

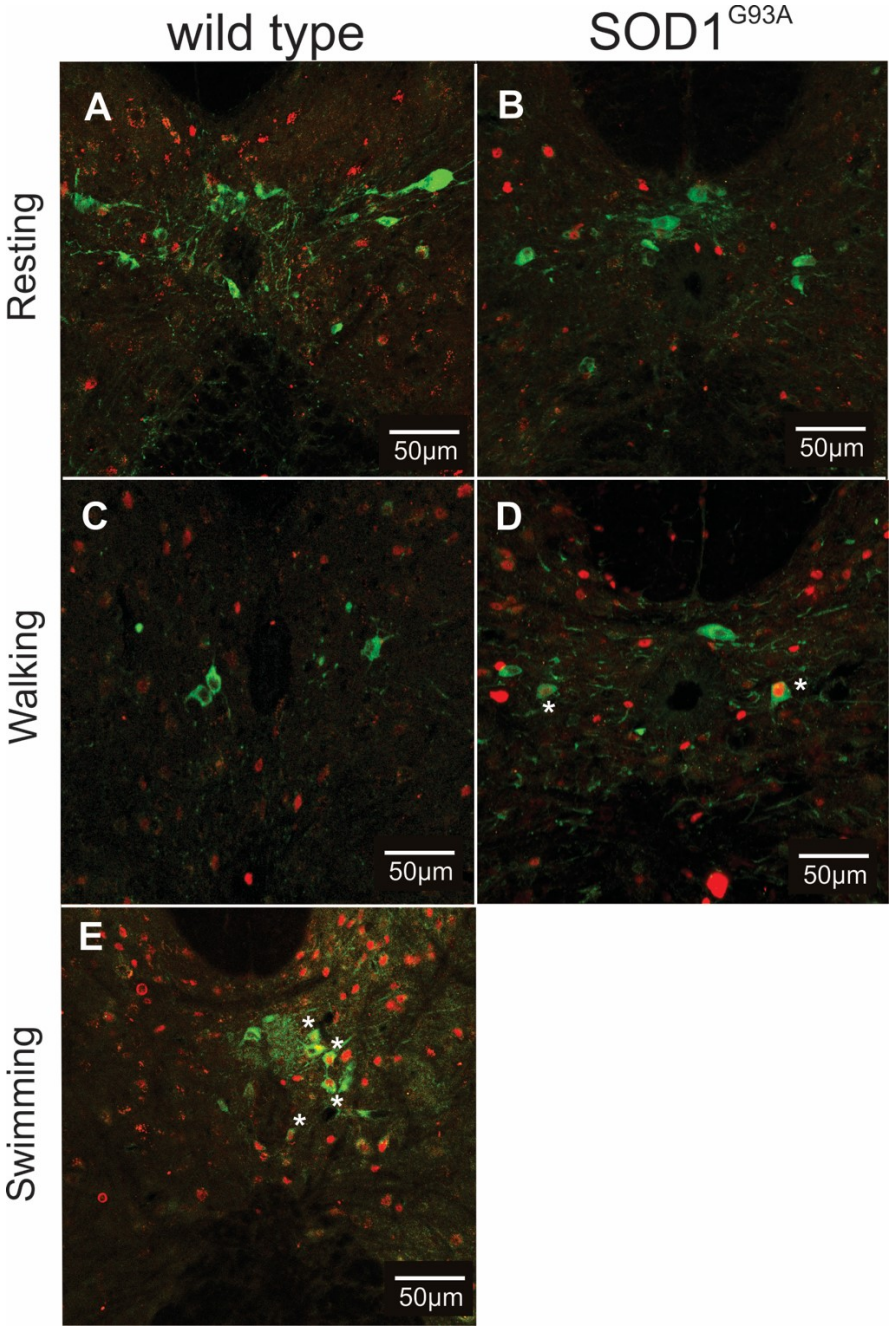

Figure 8. V0C interneurons are active in SOD1^{G93A} mice at symptomatic ages.
Activation of $V0_C$ interneurons during resting and 0.2 m/s treadmill walking was assessed in wild-type (**A** and **C**, respectively) and SOD1^{G93A} mice (**B** and **D**, respectively). $V0_C$ activation was also assessed during swimming in wild-type mice only (**E**). $V0_C$ interneurons were identified using immunohistochemistry for choline acetyl transferase (ChAT, green) and location in the vicinity of the central canal. Co-labelling of ChAT and c-fos (marker of neuronal activity, red) in neurons surrounding the central canal indicates activation of putative $V0_C$ interneurons and is marked with a blue asterisk. Note that $V0_C$ interneurons are active during walking in SOD1^{G93A} mice and during swimming in wild-type mice with no activation during walking in wild-type mice or in resting conditions.

interneurons in either WT or SOD1^{G93A} mice (Figure 8A, B). The number of putative V0$_C$ interneurons in each spinal cord section of L3-4 ranged from zero to six. In L3-4 spinal cord sections from P>100 WT mice in the walking condition, c-fos activity in putative V0$_C$ interneurons was largely absent, though one to two putative V0$_C$ interneurons were active overall per animal (Figure 4C). In spinal cord sections from P>100 SOD1^{G93A} mice in the walking condition we observed c-fos activity in one or more of the putative V0$_C$ interneurons in the majority of L3-4 spinal cord sections that we analyzed (Figure 8D). Following swimming, c-fos activity was observed in a large proportion of the putative V0$_C$ interneurons in WT mice (Figure 8E). This is the first time that V0$_C$ interneuron activity has been directly shown during swimming. Previously, the involvement of C-boutons in upregulating Gs activity during swimming was inferred from a deficit in the Gs swimming:walking activity ratio in C-bouton silenced mice (Zagoraiou et al., 2009), but was never directly shown. Based on our preliminary and qualitative analysis of V0$_C$ interneuron activity during walking, C-boutons appear to become active during walking in SOD1^{G93A} once denervation has become progressed.

3.6 SOD1^{G93A} Mice with Silenced C-Boutons Display Altered Locomotor Phenotypes

To determine whether silencing the C-boutons had an effect on the onset and nature of gait changes during disease progression in SOD1^{G93A} mice we analyzed the locomotion of WT, SOD1^{G93A}, and SOD1;C^{OFF} mice. The range of motion about the hip, knee, and ankle joints was measured during treadmill walking in conjunction with gait parameters including: stride length, step duration, swing duration, and stance duration. We also assessed the maximal treadmill speed that mice of each genotype could maintain for at least 8 steps without lagging to the back of the

treadmill. Notably, there is no ROM or gait parameter data for P>140 in the SOD1;C^{OFF} mice as they were no longer able to maintain treadmill walking at 0.2m/s.

3.6.1 SOD1^{G93A} Mice with Silenced C-Boutons Display Earlier Changes in Ankle ROM

The range of motion (ROM) about the hip, knee, and ankle joints was measured in WT, SOD1^{G93A}, and SOD1;C^{OFF} mice to determine how ALS disease progression affects movement capabilities in SOD1^{G93A} mice with and without C-bouton modulation. Statistical analyses of ROM values for each age grouping were made in comparison to the first age grouping (P40-59) within the same genotype only. There were minimal, non-significant changes the in hip ROM throughout all ages of SOD1^{G93A} and SOD1;C^{OFF} mice examined (Figure 9A). In WT mice, the hip ROM decreases in small increments until becoming statistically significant in the P110-119 age group, followed by a recovery of ROM to near starting values in the P120-139 and P>140 age groups (Figure 9A). Hip ROM tended to be increased in SOD1^{G93A} and SOD1;C^{OFF} mice compared to WT mice at all ages after P60, but these increases never reached statistical significance. There were no significant changes or obvious trends in the knee ROM within or between WT and SOD1;C^{OFF} mice at all ages (Figure 9B). In contrast, there was a trend for the knee ROM of SOD1^{G93A} mice to increase from P40-119 before beginning to decrease at P120-139 and reaching baseline values at P>140. Knee ROM in SOD1^{G93A} mice was significantly increased from P40-60 baseline values at P80-99, P100-119, and P120-139 (Figure 9B). Ankle joint ROM was most severely affected by disease progression in the SOD1^{G93A} and SOD1;C^{OFF} mice. Ankle ROM decreased slowly from week-to-week in WT mice until P100-119 (significant at P80-99, P100-119), and began to steadily increase for the remainder of the experiment (Figure 9C). Significant decreases in ankle ROM occur in SOD1^{G93A} mice at P100-119 and P120-139 with a slight recovery

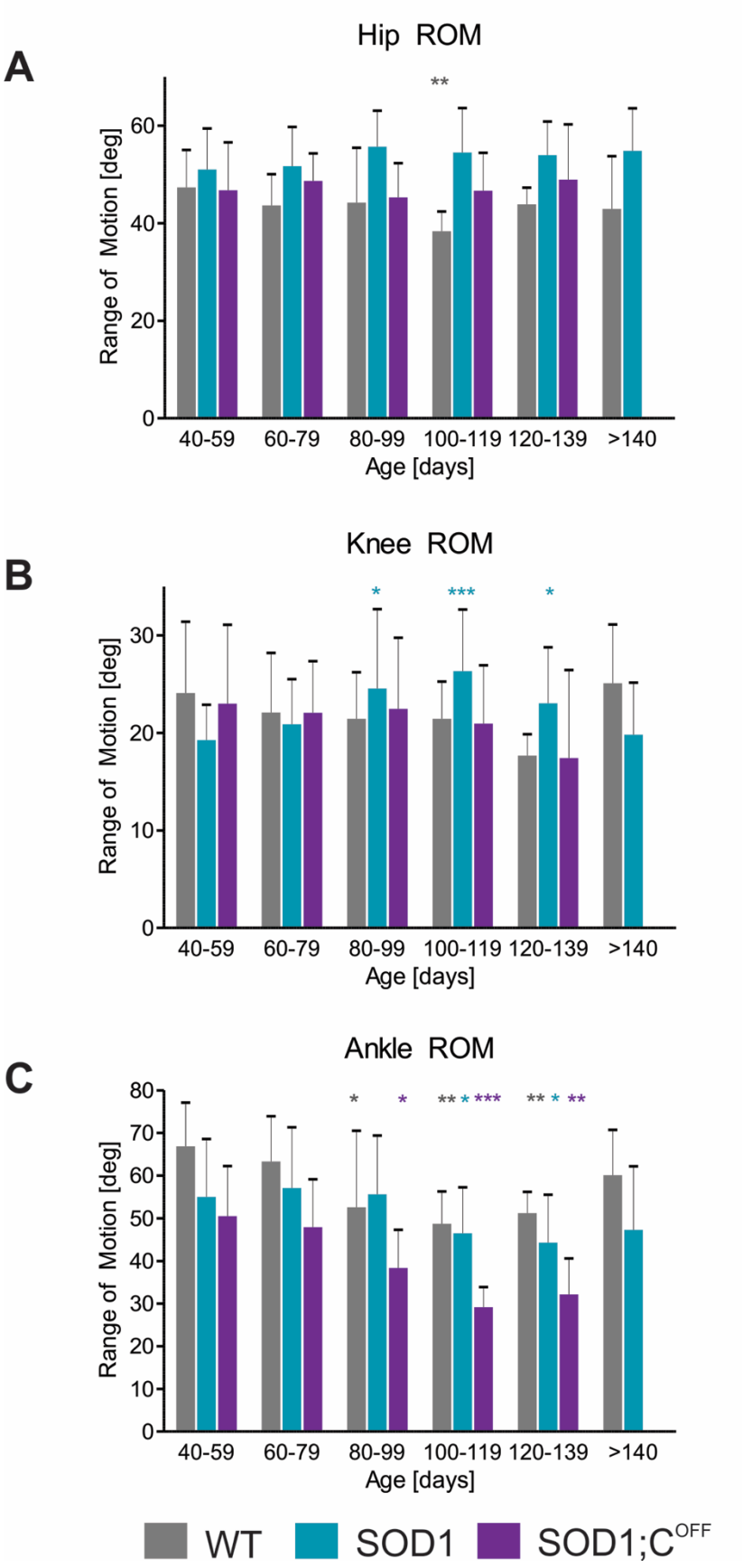
A
Hip ROM
**
Range of Motion [deg]
0
20
40
60
40-59
60-79
80-99
100-119
120-139
>140
Age [days]
B
Knee ROM
*
***
*
Range of Motion [deg]
0
10
20
30
40-59
60-79
80-99
100-119
120-139
>140
Age [days]
C
Ankle ROM
* * ** * *** ** * **
Range of Motion [deg]
0
10
20
30
40
50
60
70
80
40-59
60-79
80-99
100-119
120-139
>140
Age [days]
WT
SOD1
SOD1;C^OFF

Figure 9. Ankle ROM becomes significantly reduced with disease progression in SOD1^{G93A} and SOD1;C^{OFF} mice

Hip (**A**), knee (**B**), and ankle (**C**) ROM was assessed in wild-type, SOD1^{G93A} and SOD1;C^{OFF} mice. Statistical difference over time was assessed within each genotype by comparing each age group to the P40-59 age group. No comparisons were made between genotypes. Statistical differences were tested with either a Student's t-test or a Mann-Whitney test depending on whether normality was achieved. *$p<0.05$, **$p<0.01$, and ***$p<0.001$. Pooled data was obtained from n=6 wild-type mice, n=13 SOD1^{G93A} mice, and n=5 SOD1;C^{OFF} mice.

of ROM at P>140 (Figure 9C). SOD1;C^{OFF} mice had a decreased ankle ROM at all ages compared to WT and $SOD1^{G93A}$ mice. Significant decreases in ankle ROM began at P80 in SOD1;C^{OFF} mice and did not recover by P139 when mice were no longer able to walk on the treadmill at 0.2m/s (Figure 9C). Overall, there were minimal changes in range of motion about the hip and knee joints in WT, $SOD1^{G93A}$, and SOD1;C^{OFF} mice from P40 until P>140 (Figure 9A, B). In contrast, ankle ROM became progressively smaller in $SOD1^{G93A}$ and SOD1;C^{OFF} mice with disease progression beginning at P100-119 and P80-99, respectively (Figure 9C). Interestingly, we observed the onset of TA bursting and ankle joint fluctuations during the swing phase occurred on average at P68.2 (±7.66 SD) in SOD1;C^{OFF} mice, but not until P 83.87 (±3.18 SD) in $SOD1^{G93A}$ mice. Loss of ankle joint mobility can cause changes in foot placement during locomotion that can result in changes in gait parameters such as the stride length, stride duration, swing duration, and stance duration.

3.6.2 Silencing the C-boutons Produces Earlier Gait Changes in $SOD1^{G93A}$ Mice

To determine whether silencing the C-boutons affected the timing and nature of the onset of locomotor disturbances in $SOD1^{G93A}$ mice, changes in gait were monitored in WT, $SOD1^{G93A}$, and SOD1;C^{OFF} mice walking at 0.2m/s using measurements of stride length, step duration, swing duration, and stance duration. It was predicted that silencing of the C-boutons would cause changes in gait to occur earlier in SOD1;C^{OFF} mice than in $SOD1^{G93A}$ mice with functional C-boutons. Statistical analyses of gait parameters for each age grouping were made in comparison to the first age grouping (P40-59) within the same genotype only.

Stride length is a measurement of the distance between the location of the paw at the beginning and end of stance phase. In WT mice, stride length was highly variable at early ages,

but showed a general trend to increase with age. At P100-119 there was a significant decrease in stride length in WT mice, but stride length increased with age from this point and was significantly increased at P>140 (Figure 10A). Stride length was significantly increased in $SOD1^{G93A}$ mice at P80-99, but steadily declined (though not significantly) from P100 to P>140 (Figure 10A). Although none of the changes in stride length reached statistical significance for $SOD1;C^{OFF}$ mice, stride length was decreased at P80 and became progressively shorter with age (Figure 10A). In order to maintain the treadmill speed of 0.2m/s when the stride length is shortening, mice would have to take more frequent steps that are shorter in duration.

Step duration, or cycle period, is the length of time between the beginning of two consecutive swing phases. Step duration was relatively constant at all ages in WT mice with a slight, non-significant increase seen at P>140 (Figure 10B). As with the changes in stride length in $SOD1^{G93A}$ mice, step duration was significantly increased at P80-99, but became gradually shorter beginning at P100 and reaching significance at P>140 (Figure 10B). There was a significant decrease in the step duration of $SOD1;C^{OFF}$ mice at P80 that was maintained until P139 (Figure 10B). Step duration can be further broken down into the duration of the swing and stance phases.

Swing duration is the portion of the step cycle time that is spent in swing phase. In WT mice, the swing phase duration is significantly shorter from P80-139 and increases slightly at P>140 (Figure 10C). Swing duration increases slightly in $SOD1^{G93A}$ mice at P80-99 before becoming significantly decreased at P120-139 and further decreased at P>140 (Figure 10C).

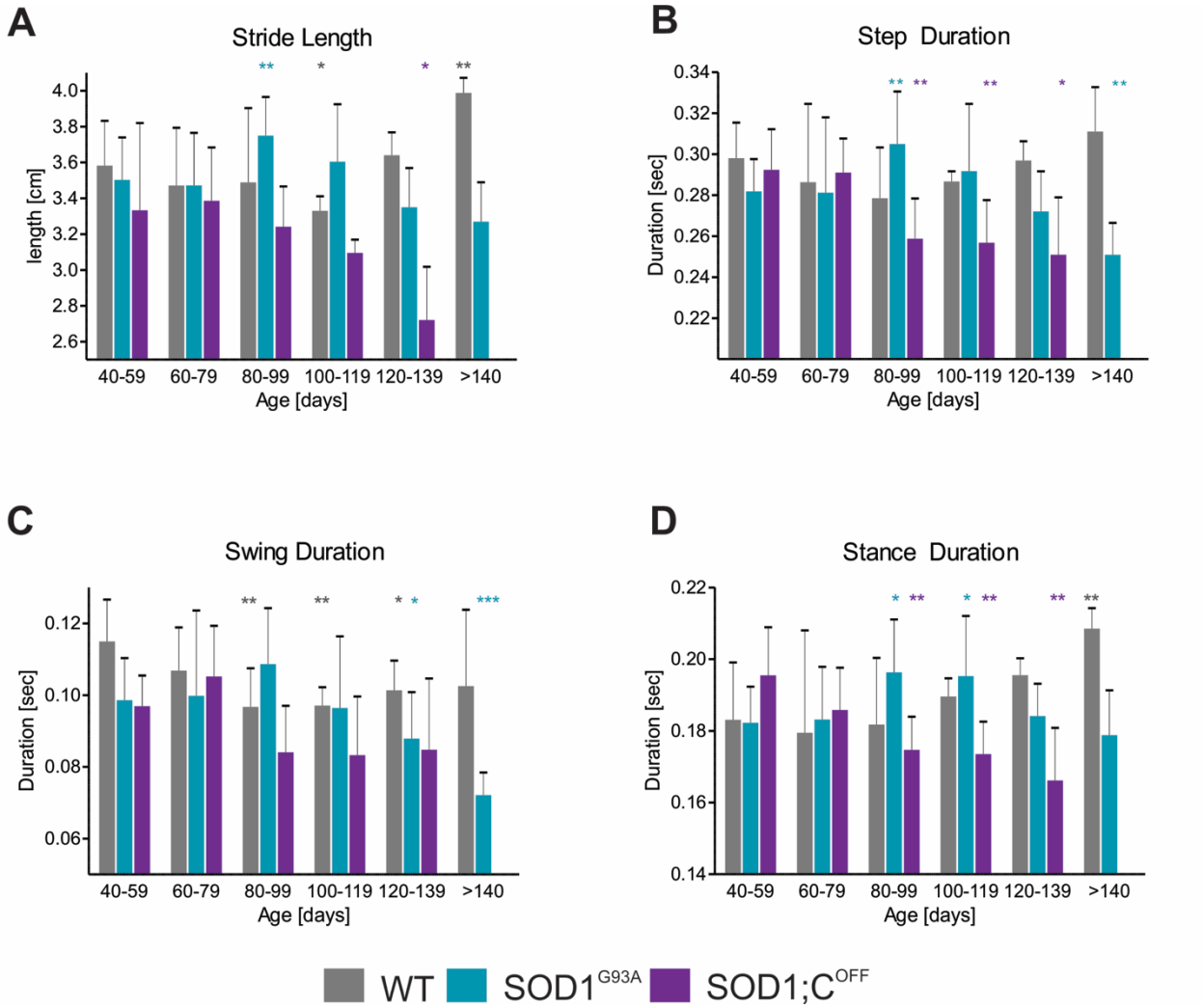

Figure 10. Changes in gait throughout disease progression in SOD1^{G93A} mice with and without functional C-boutons.
Stride length (**A**), step duration (**B**), swing duration (**C**), and stance duration (**D**) were assessed in wild-type, SOD1^{G93A} and SOD1;C^{OFF} mice. Statistical difference over time was assessed within each genotype by comparing each age group to the P40-59 age group. No comparisons were made between genotypes. Statistical differences were tested with either a Student's t-test or a Mann-Whitney test depending on whether normality was achieved. *p<0.05, **p<0.01, and ***p<0.001. Pooled data was obtained from n=6 wild-type mice, n=9 SOD1^{G93A} mice, and n=5 SOD1;C^{OFF} mice.

In SOD1;C^{OFF} mice, there is a non-significant decrease in duration of the swing phase at P80-99 that is maintained until the end of the experiment (Figure 10C).

Stance duration is the portion of the step cycle time that is spent in stance phase. The stance duration of WT mice begins to gradually increase beginning at P80-99 and becomes significantly longer by P>140 (Figure 10D). For $SOD1^{G93A}$ mice, the changes in stance duration parallel the changes in the previous three gait parameters. There is a significant increase in stance duration from P80-119 followed by a slight decline beginning at P120 which dropped slightly below baseline at P>140 (Figure 10D). In SOD1;C^{OFF} mice, the changes in stance phase duration also follow the trends of the previous three gait parameters. The duration of the stance phase begins to decline at P60-79 and is significantly shorter at P80-99 with further decreases with age until the end of the experiment (Figure 10D).

Overall, on all four gait parameters measured, there are trends in the gait parameter changes unique to each genotype. WT mice tended to show initial decreases on the gait parameters that uniformly began to increase at P120-139. The trend in $SOD1^{G93A}$ mice is opposite to that of the WT mice. In $SOD1^{G93A}$ mice, strides become longer and step, stance, and swing durations are increased until P80-99 before beginning to decrease at P100 and reaching below baseline by P>140. In SOD1;C^{OFF} mice, all gait parameters decrease at P80-99 and either remain constant or further decrease until P139 when mice are no longer able to keep up with the treadmill at 0.2 m/s. $SOD1^{G93A}$ mice were able to keep up with the treadmill at 0.2 m/s until ~P155.

3.6.3 SOD1^{G93A} Mice with Silenced C-Boutons Display Earlier Deficits in Maximal Speed

We assessed the maximal treadmill speed that mice of each genotype were able to keep up without lagging to the back of the treadmill. On average, mice of all genotypes are able to keep up with a treadmill speed of 0.4 m/s until P100-119. The average maximal treadmill speed for WT mice increases gradually with age until reaching a maximum of 0.6 m/s that is uniformly achieved by all WT mice at and beyond P120 (Figure 11). In SOD1^{G93A} mice, average maximum treadmill speed increases slowly with age until reaching speed of 0.5 m/s at P100-119 which all SOD1^{G93A} mice at this age are capable of. Beginning at P120-139 average max speed begins to decrease in SOD1^{G93A} mice and drops below 0.2 m/s at P>140. SOD1;C^{OFF} mice have the earliest and largest decreases in average maximal treadmill speed. Average maximal treadmill speed begins to decline in SOD1;C^{OFF} mice at P100-119 and drops significantly with age beginning at P120. The average maximal speed of SOD1;C^{OFF} mice at P>140 is only 0.064 m/s.

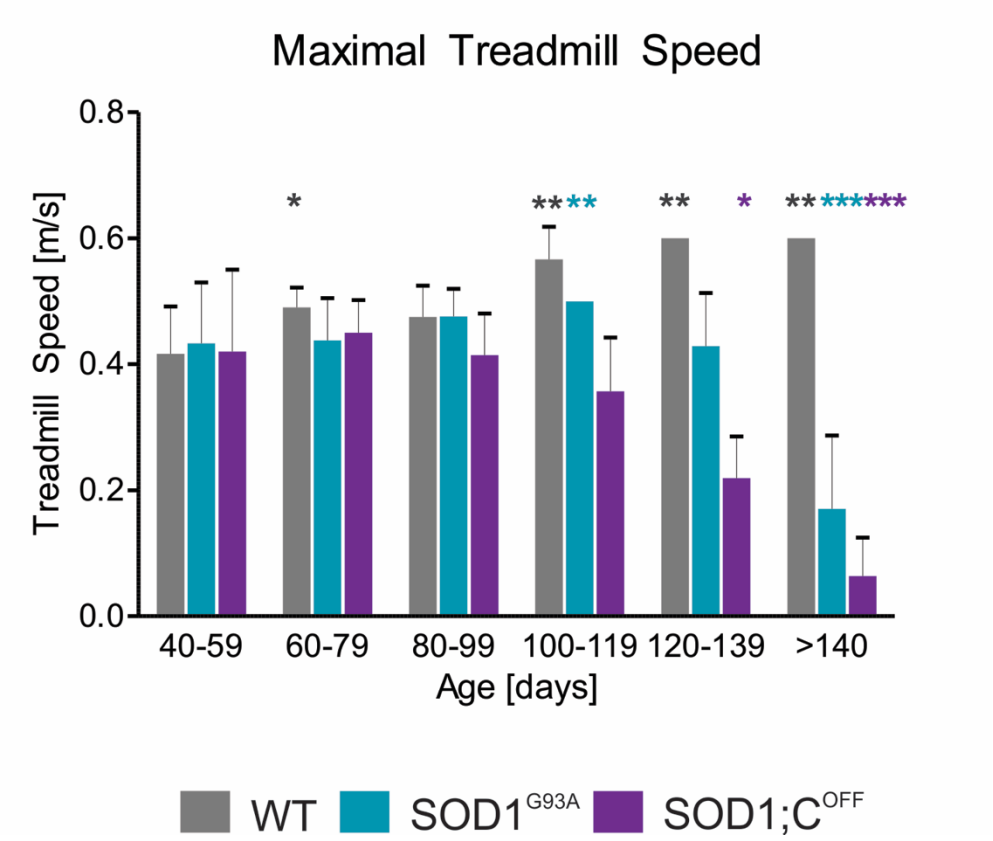

Figure 11. Silencing of C-boutons accelerated deficits in maximal treadmill speed in SOD1^{G93A} mice

The maximal treadmill speed, the fastest speed that mice could maintain without lagging to the back of the treadmill, was assessed in wild-type, SOD1^{G93A}, and SOD1;C^{OFF}. Note the earlier decrease in treadmill speed in SOD1;C^{OFF} mice compared to SOD1^{G93A} mice. The absence of error bars indicates that all mice in that age group had the same maximal speed. Statistical differences were tested with either a Student's t-test or a Mann-Whitney test depending on whether normality was achieved. *p<0.05, **p<0.01, and ***p<0.001. Pooled data was obtained from n=6 wild-type mice, n=13 SOD1^{G93A} mice, and n=5 SOD1;C^{OFF} mice.

CHAPTER 4: DISCUSSION

4.1 Summary of Key Findings

The first aim of this project was to characterize the disease progression in our colony of $SOD1^{G93A}$ mice. Denervation began in the Gs and TA at ~P60 and ~P70, respectively. By end-stage (P169), muscle innervation was 13% in the Gs and ~20% in the TA (Figure 2B, D). Denervation did not begin in the Sol muscle until ~P110, but increased steadily until innervated NMJs were detected at <20% at P160 (Figure 2F). To measure denervation in individual mice across time, muscle innervation was investigated indirectly by measuring changes in CMAP. The Gs CMAP was shown to decrease to ~50% of the maximum at ~P90-100 and decline slowly until reaching ~15% at end-stage (Figure 3). Despite changes in muscle innervation by ~P60-70, $SOD1^{G93A}$ mice did not show any changes in locomotion until ~P84 when the TA activity became bursty and the ankle angle began to fluctuate during swing phase (Figure 4B, D). At ~P90, $SOD1^{G93A}$ mice began to show deficits in upregulation of Gs muscle activity during swimming and the swimming:walking ratio of Gs activity was ~2 or less (Figure 5C, Figure 6B, D). Cholinergic modulation of surviving motor neurons through the C-boutons was hypothesized to be involved in compensating for motor unit loss. Immunohistochemistry using c-fos showed that putative $V0_C$ interneurons, the neuronal source of C-boutons, were active during walking in $SOD1^{G93A}$ mice but not WT mice after ~P100. $V0_C$ interneurons were also directly shown to be active in WT mice during swimming for the first time. The onset of TA bursting and ankle joint fluctuations during the swing phase occurred at P68.2 (±7.66 SD) in $SOD1;C^{OFF}$ mice, but not until P83.87 (±3.18 SD) in $SOD1^{G93A}$ mice. Ankle ROM became significantly decreased in $SOD1;C^{OFF}$ mice earlier than in $SOD1^{G93A}$ mice (Figure 9C). Furthermore, $SOD1;C^{OFF}$ mice began to show gait deficits at P80-99, but this was not observed in $SOD1^{G93A}$ mice until P100-119 (Figure

10 A-D). Finally, deficits in maximal treadmill speed become apparent in SOD1;C^{OFF} mice at P100-119 and in $SOD1^{G93A}$ mice at P120-139. Based on these observations, C-bouton modulation of motor neurons is important for behavioural compensation after motor unit loss in ALS.

4.2 Compensation for Motor Unit Loss is Occurring during ALS Disease Progression

4.2.1 Motor Unit Loss in ALS Patient and $SOD1^{G93A}$ Mice

Muscle denervation and motor unit loss are central to the development of muscle weakness and paralysis during ALS disease progression. Through the use of histology in ALS research, a significant amount of knowledge regarding the onset of motor neuron dysfunction and the timeline of muscle denervation has been created (Fischer et al., 2004; Frey et al., 2000; Gould et al., 2006; Mead et al., 2011; Pun et al., 2006; Vinsant, Mansfield, Jimenez-Moreno, Del, et al., 2013). However, one limitation of using histology to investigate muscle denervation is that histology is only capable of providing one data point from each animal at a singular point in time. ALS is recognized to be a highly individualized disease and muscle innervation is a dynamic process wherein denervated muscle fibers can be reinnervated by collateral axon sprouts (Schaefer, Sanes, & Lichtman, 2005). Therefore, we sought to characterize muscle denervation in individual $SOD1^{G93A}$ mice from pre-symptomatic stages to end-stage of the disease using an *in vivo* methodology that indirectly measures denervation by monitoring of changes in the CMAP. Net increases in the CMAP represent an increase in the number of functional motor units whereas net decreases represent a decrease in number of functional motor units. The benefit of using CMAP instead of histology to assess muscle innervation is that it allows the longitudinal study of individual animals and when performed in conjunction with kinematic and EMG recordings of

motor behaviour, as was done in this study, direct inferences about the effects of muscle denervation on behaviour and motor function can be made.

Using CMAP to monitor the loss of functional motor units in SOD1^{G93A} mice, we found that Gs CMAP drops to ~50% of the maximum at ~P90-100 followed by a slower, steadier decline of the CMAP until end-stage of the disease (Figure 3 E, F, H). However, in one animal there was an increase in the Gs CMAP beginning at P134 that was maintained until end-stage at P169 (Figure 3G). One possible explanation for the increase of CMAP is the collateral reinnervation of previously denervated motor end plates by sprouts from nearby surviving motor neurons. The Gs CMAP at P169 in this mouse was ~85% of the maximum, but the hind-end was completely paralyzed and the mouse was euthanized later that day due to an inability to right itself. Therefore, it is unlikely that the CMAP increase was due to collateral reinnervation because this would imply an increase in functional motor units when the animal was evidently paralyzed. A more likely explanation may be that the electrode was displaced from the muscle and the activity that was picked up by the electrode was non-specific.

To determine the validity of using CMAP as an indirect measurement of muscle denervation, we compared the timeline of Gs CMAP changes to muscle denervation data obtained using histology. Histological measures of Gs muscle denervation show that denervation began at ~P60 and plateaued at ~50% from P70-P110 before muscle innervation slowly declined to only 13% at P169. However, three data points from P100-P125 place innervation of the Gs at greater than 80% in SOD1^{G93A} mice (Figure 2B). As this is approximately half of the animals that were analyzed for that time period, the number of animals will have to be increased to determine with

certainty the level of Gs innervation at this stage and to confirm that denervation onset is at ~P60 in SOD1^{G93A} mice and not after P125. Therefore, histology is preliminarily a more sensitive method than CMAP for detecting early changes in denervation in SOD1^{G93A} mice. However, beyond P100 the changes in CMAP very closely parallel the changes in Gs innervation observed using histology.

Our analysis of NMJ innervation of the Gs, TA, and Sol muscles showed some similarities to previous reports using high-expresser SOD1^{G93A} mice. Overall, denervation of the fast-twitch Gs and TA muscles occurred earlier than the slow-twitch Sol muscle (Figure 2B, D, F). This is in agreement with the previously reported selective vulnerability of FF and FR motor units and the relative resiliency of S motor units to disease-associated loss (Atkin et al., 2005; Frey et al., 2000; Hegedus et al., 2007; Mead et al., 2011; Vinsant, Mansfield, Jimenez-Moreno, Moore, et al., 2013). Mead et al. previously reported that innervation of the Gs was 40% at P60 (Mead et al., 2011), whereas we report Gs innervation of 34% at P60, but 50% from P70-P110 (Figure 2B). The variation in Gs innervation from P60 to P70 may indicate that the P60 mouse was progressing particularly fast and highlights the importance of being able to track muscle denervation in individual animals. Innervation of the TA muscle was previously reported to be 60% at P30 and 30% by P100 (Vinsant, Mansfield, Jimenez-Moreno, Moore, et al., 2013). However, we did not observe any changes in TA innervation until P70 when innervation was 60%. From P70-P130 TA innervation ranged from 40-60% followed by a decrease to 20% at P169 (Figure 2D). Vinsant et al. reported that there are no changes in Sol muscle innervation at P30 and only a slight, insignificant decrease in innervation at P100 (Vinsant, Mansfield, Jimenez-Moreno, Del, et al., 2013). We also did not observe any large deviations in Sol muscle innervation in SOD1^{G93A} mice

compared to WT mice at P30 or P100. However, at P110 Sol innervation began to gradually decline until end-stage of the disease (~P150-P170) when we report Sol innervation of less than 20% (Figure 2F). Overall, denervation of the Gs, TA, and Sol muscles in our colony of high-expresser SOD1^{G93A} mice does not appear to progress as quickly as in previous reports. Although the phenotype of SOD1^{G93A} mice is known to be variable between laboratories using identical strains (Kanning et al., 2010), it is also possible that our mice express a different copy number of the SOD1^{G93A} gene or are on a different genetic background than the mice used in the previous reports. The number of gene copies and the genetic background of SOD1^{G93A} mice has previously been shown to influence the disease progression and could explain the variation in reports of muscle denervation between studies (Gurney et al., 1994; Nardo et al., 2016).

4.2.2 Behavioural Phenotypes in SOD1^{G93A} Mice

We recorded kinematic and EMG data simultaneously during treadmill locomotion in WT and SOD1^{G93A} mice to determine how changes in muscle activity relate to changes in movement. Despite muscle denervation of ~50% in the Gs and 40-60% in the TA of SOD1^{G93A} mice by P100, there were remarkably small changes in motor phenotype. The earliest detectable abnormality in muscle activity during locomotion was observed at ~P84 when the TA activity profile during swing phase changed from a large singular burst to multiple small bursts which caused fluctuations of the ankle angle that approximately coincided with each burst (Figure 4B, D). The ROM of the ankle was significantly reduced in SOD1^{G93A} mice at P100-119 compared to the starting point (Figure 9C), whereas ankle ROM was previously reported to decrease beginning at ~P80 (Preisig et al., 2016). The fluctuations in ankle angle caused by repetitive bursting of the TA muscle as the leg moves through swing phase occurs ~16 days prior to changes in ankle ROM and may represent

early deficits in ankle flexion that eventually progress to a significant reduction in ankle ROM. A more limited range of motion about the ankle joint influences how far forward or backward the paw is located at the beginning and end of swing phase, respectively, and can therefore produce shortened strides. In $SOD1^{G93A}$ mice, stride length was shown to decrease, though not significantly, between P120 and P>140 (Figure 10A) which is later than previous reports that observed a shortened stride length at ~P90-P120 (Gurney et al., 1994; Mead et al., 2011; Preisig et al., 2016). The duration of the stance phase is increased in $SOD1^{G93A}$ mice from P80-P119, but begins to decrease at P120 (Figure 10D). One previous study also reported an increase in stance phase duration at P90 (Mancuso et al., 2011), whereas other studies have reported this at ~P60 (Wooley et al., 2005). The increase in stance phase and stride length in $SOD1^{G93A}$ mice beginning at P80 likely represents a deficit in pushing off during the propulsion phase of stance that becomes progressively more difficult with increases in muscle weakness. In contrast, the decrease in the stance phase duration beginning at ~P120 is paralleled by a decrease in stride length and ankle ROM which suggests that the decrease in stance time is due to a loss of ankle ROM that produces shorter strides. As the disease progresses in $SOD1^{G93A}$ mice, the loss of ankle ROM and accumulating changes in gait lead the decreases in the maximal treadmill walking speed. The $SOD1^{G93A}$ mice in this study were able to walk on the treadmill at 0.5m/s until P119. After P119, speed gradually decreased until end-stage (~P150-P170) when $SOD1^{G93A}$ mice were only capable of speeds below 0.1m/s (Figure 11). However, a previous study reported that $SOD1^{G93A}$ mice were unable to walk at speeds above 0.2m/s by ~P120 (Mancuso et al., 2011). Overall, the onset of gait parameter changes, decreases in ankle ROM, and decline in maximal treadmill speed tend to occur later in our colony of $SOD1^{G93A}$ mice than in previous reports, which is consistent with our reports of comparable levels of denervation at later ages.

4.2.3 Motor Unit Loss Precedes Onset of Motor Dysfunction

The onset of motor unit loss occurs far before any changes in motor function or muscle strength in ALS patients and SOD1^{G93A} mice. When ALS patients seek medical care regarding changes in muscle strength and movement, they have already lost up to 50% of their motor units (McComas et al., 1971). In SOD1^{G93A} mice, we analyzed EMG activity and kinematics during locomotion and assessed changes in ROM and four different gait parameters and the earliest abnormality that we could detect occurred at P84 (Figure 4B, D), approximately 15-25 days after significant denervation of the Gs and TA muscles. Based on these reports, the occurrence of compensation for motor unit loss is evident in ALS patients and SOD1^{G93A} mice, yet remarkably little is known about the mechanisms underlying compensation.

4.3 C-Bouton Modulation of Motor Neurons Compensates for Motor Unit Loss in ALS

4.3.1 Proposed Mechanism of Compensation

For SOD1^{G93A} mice to maintain normal movement despite motor unit loss, the output of the motor pool after motor unit loss must be equal to the output before motor unit loss. Motor output can be modified by changing the number and size of motor units recruited or by changing the firing frequency of active motor neurons. Progressive motor neuron loss is occurring in ALS, beginning with the large motor units, making it unlikely that motor output is maintained by recruiting more motor neurons. Therefore, motor output is likely maintained by increasing the firing frequency of surviving motor neurons. C-bouton modulation of motor neurons was proposed here as a potential compensatory mechanism based on their previously shown ability to increase the firing frequency of motor neurons by reducing the after-hyperpolarization (Miles et al., 2007).

C-boutons have also been shown to be enlarged on motor neurons in SOD1^{G93A} mice at pre-symptomatic stages and C-bouton loss is reported in SOD1^{G93A} mice and ALS patients at end-stage (Chang & Martin, 2009; Lasiene et al., 2016; Nagao et al., 1998). Therefore, we hypothesized that "cholinergic modulation of motor neurons through the C-boutons increases the excitability of surviving motor neurons to compensate for motor unit loss during ALS disease progression."

4.3.2 SOD1^{G93A} Mice Lose the Ability to Modulate Gs Activity with Disease Progression

C-boutons are known to be involved in the upregulation of Gs activity during swimming compared to walking (Zagoraiou et al., 2009). We found that SOD1^{G93A} mice upregulated Gs activity during swimming compared to walking at pre-symptomatic ages (P<90) (Figure 5B). However, SOD1^{G93A} mice lost the ability to upregulate Gs activity during swimming after P90 and similar amplitudes of Gs activation were observed during swimming and walking (Figure 5C). A swimming:walking ratio of Gs activity was calculated to quantitatively assess task-dependent changes in Gs amplitude. In WT mice, there were no age related changes in the Gs activity ratio, but there were large fluctuations throughout (Figure 6A, C). Although it is difficult to know what caused these fluctuations, one possible explanation is changes in the swimming speed from week to week, though this was not measured here. In SOD1^{G93A} mice, there is remarkably little fluctuation in the Gs activity ratio and at ~P90 there is a systematic decline in the ratio to below 2 in almost all animals. The CMAP was observed to decrease to ~50% of the maximum at ~P90-100 in SOD1^{G93A} mice, suggesting a large loss of functional motor units. The concomitant drop in CMAP and Gs swimming:walking activity ratio is consistent our hypothesis that C-bouton modulation is involved in compensation. The drop in CMAP indicates that motor unit loss has occurred, and suggests that cholinergic modulation of motor neurons will increase to compensate

for motor unit loss, thereby producing normal behaviour during walking. However, the extra boost in motor neuron excitability provided by the C-boutons during walking results in a lack of further excitability that can be provided to motor neurons during swimming (Figure 7C, D), which leads to a decrease in Gs swimming:walking activity ratio.

4.3.3 Walking Induces $V0_C$ Interneuron Activity in Symptomatic $SOD1^{G93A}$ Mice

Using c-fos immunohistochemistry, we demonstrated that $V0_C$ interneurons, the neuronal source of C-boutons, are active during walking in $SOD1^{G93A}$ mice after P100 (Figure 8D). This observation directly supports our hypothesis that once a significant portion of motor units are lost, $V0_C$ interneuron activity is upregulated to increase motor neuron excitability through the C-boutons and produce normal walking behaviour. We also provided the first direct evidence of $V0_C$ activity during swimming (Figure 8E). Previously, the involvement of C-boutons in upregulating Gs activity during swimming was inferred from a deficit in the Gs swimming:walking activity ratio in C-bouton silenced mice (Zagoraiou et al., 2009), but was never directly shown. Our observations of c-fos activity in ChAT positive neurons are purely qualitative and future analysis should systematically quantify the number of c-fos positive, ChAT positive neurons in the vicinity of the central canal under each condition. There are no specific immunohistochemistry markers for $V0_C$ interneurons, but putative $V0_C$ interneurons are identified by ChAT expression and location in the vicinity of the central canal in lamina X. A limitation of these experiments is that the distribution of c-fos expression has not been analyzed to determine whether specific patterns of activation associated with different forms of locomotion can be reliably detected using c-fos and to rule-out the possibility of random activity.

4.3.4 Silencing of C-Boutons in SOD1^{G93A} Mice Impairs Compensation

We were able to silence the C-boutons in SOD1^{G93A} mice using the *SOD1^{G93A};Dbx1::Cre;Chat$^{fl/fl}$* mouse line. Owing to the low yield of animals with *SOD1^{G93A}, Cre* recombinase, and *Chat$^{fl/fl}$*, we were unable to further select for exclusively males as was done for the SOD1^{G93A} experiments to avoid gender differences. Four of the five mice used for the SOD1;C^{OFF} experiments were female and only one was male. As a result, some of the comparisons between SOD1^{G93A} mice and SOD1;C^{OFF} mice may be influenced by gender differences.

The earliest symptoms of motor dysfunction in SOD1;C^{OFF} mice were the onset of TA bursting and ankle joint fluctuations during swing phase. This occurred in all four female SOD1;C^{OFF} animals at ~ P63 which is 21 days earlier than in SOD1^{G93A} mice (~P84). However, the bursty TA onset occurred in the male SOD1;C^{OFF} mouse at P81 which is nearly the same time as SOD1^{G93A} mice. As we had no other male mice to compare with, it is unclear whether earlier onset of TA bursting is the result of gender differences or related to silencing of the C-boutons. However, the behaviour of the male SOD1;C^{OFF} mouse was qualitatively very similar to the behaviour of the female SOD1;C^{OFF} mice.

SOD1;C^{OFF} mice develop a significant decrease in ankle joint ROM ~20 days earlier (P80-99) than SOD1^{G93A} mice (P100-119) (Figure 9C). The onset of TA bursting and fluctuations in ankle movement precede the decrease in range of motion by ~20 days in SOD1;C^{OFF}mice and ~16 days in SOD1^{G93A} mice. This very precise delay of ~2-3weeks from the onset of the bursty TA activity profile to the development of a significant decrease in ROM suggests that onset of TA bursting can accurately predict the onset of subsequent ankle ROM changes. In SOD1;C^{OFF} mice,

the step duration and stance duration are significantly decreased and the swing duration and stride length are decreased, though not significantly, at P80-99 (Figure 10A-D). Silencing of the C-boutons in SOD1;C^{OFF} mice results in an inability to compensate for motor unit loss leading to a significant decrease in ankle ROM at P80-99. The decrease in ankle ROM directly influences the positioning of the paw at the beginning and end of swing phase which translates to a decrease in stride length. When stride length decreases while mice are walking at a constant speed, the step duration will also decrease as animals take quicker, more frequent steps to keep up with the treadmill. While the swing and stance durations are both reduced in SOD1;C^{OFF} mice at P80-99, only the reduction in the stance phase reaches statistical significance, indicating that the increase in stepping frequency is accomplished primarily by shortening the stance phase although the swing phase is also decreased. Interestingly, at the same age (P80-99), $SOD1^{G93A}$ mice have the exact opposite set of gait parameters. The step duration, stance duration, and stride length are significantly increased and the swing duration is increased, though not significantly (Figure 10A-D). The direct opposite trends in gait parameters in the $SOD1^{G93A}$ mice and the SOD1;C^{OFF} mice at P80-99 demonstrates the vastly different capabilities for compensation between $SOD1^{G93A}$ mice with functional C-boutons and those without. The SOD1;C^{OFF} mice also show deficits in maximal treadmill walking speed ~20 days earlier (P110-119) than $SOD1^{G93A}$ mice (P120-139) (Figure 11), which indicates increased muscle weakness and a declining ability to propel the body forward with force and speed at P100-119 in the SOD1;C^{OFF} mice compared to $SOD1^{G93A}$ mice.

Overall, the onset of motor symptoms occurs in SOD1;C^{OFF} mice approximately 15-20 days before the onset in $SOD1^{G93A}$ mice. The bursty TA profile occurs in SOD1;C^{OFF} mice at ~P68 followed by the onset of ankle range of motion deficits and decreases in the stride length, step

duration, stance duration, and swing duration at P80-99. The onset of motor symptoms in SOD1;C^{OFF} mice at ~P68 indicates that C-boutons would normally begin to compensate for motor unit loss at this age. Therefore, without cholinergic modulation of motor neurons through C-boutons, minimal compensation for motor unit loss occurs, and the onset of motor deficits corresponds more closely to the onset of denervation in the Gs (P60) and TA (P70) muscles.

Cholinergic modulation of motor neurons through the C-boutons is shown here to compensate for motor unit loss and preserve motor function in $SOD1^{G93A}$ mouse models of ALS. While we demonstrate that C-bouton modulation of motor neurons is beneficial in terms of preserving motor function, a chronic increase in the excitability of motor neurons may also lead to motor neuron death through excitotoxicity (Herron & Miles, 2012; Witts et al., 2014). However, the two SOD1;C^{OFF} mice that have reached end-stage so far were P153 and P155 at the time of euthanasia due to severe paralysis and difficulties righting. $SOD1^{G93A}$ mice reach end-stage at P156.6 (±8.71 SD). From the few mice that we have analyzed so far, $SOD1^{G93A}$ mice and SOD1;C^{OFF} mice appear to reach end-stage at similar ages which would suggest that C-bouton activity does not negatively impact the survival rate of $SOD1^{G93A}$ mice.

4.4 Implications for Treatment of ALS Patients

Muscle weakness in the upper and lower extremities is the presenting symptom in more than 70% of human ALS patients (Dal Bello-Haas et al., 2007). Exercise has been proposed as a potential treatment for improving muscle strength and preventing muscle wasting, but the role of exercise in ALS remains controversial. The concern with prescribing exercise as a treatment in ALS is the potential to overwork the muscle through excessive exercise and strengthening (Dal

Bello-Haas et al., 2007). However, regular exercise has been shown to improve functionality and ameliorate symptoms in ALS patients (Dal Bello-Haas et al., 2007; Drory, Goltsman, Goldman Reznik, Mosek, & Korczyn, 2001; Pinto et al., 1999). The benefits of exercise on ALS have been tested in mouse models of the disease, but the results are conflicting. Regular, moderate intensity exercise has been shown to provide neuroprotection and modestly increase survival (Kaspar, Frost, Christian, Umapathi, & Gage, 2005; Kirkinezos, Hernandez, Bradley, & Moraes, 2003; Veldink et al., 2003). However, high-intensity endurance treadmill exercise in $SOD1^{G93A}$ mice has been found to increase the onset of muscle weakness and decrease survival (Mahoney, Rodriguez, Devries, Yasuda, & Tarnopolsky, 2004).

Based on the beneficial effects, or at the very least the lack of detrimental effects, of moderate intensity exercise on ALS and our observations that compensation for motor unit loss is achieved by cholinergic modulation through the C-boutons, we suggest that a therapeutic program that includes physical exercise in the form of swimming may be beneficial for ALS patients. Swimming is a low-impact form of exercise that we have shown here to activate the C-boutons. C-bouton activation through moderate exercise has the potential to preserve mobility in patients with ALS and when combined with the muscle strengthening effects of exercise may improve overall motor function and quality of life. Alternatively, C-boutons could be targeted pharmacologically to induce activity that would increase motor neuron excitability to functionally compensate for ongoing motor unit loss. One caveat is that C-boutons loss has been reported at post-mortem autopsy of human ALS patients (Nagao et al., 1998) which indicates that C-boutons may also be susceptible to degeneration in ALS and the therapeutic activation of C-boutons to preserve motor function may only be applicable during earlier stages of the disease.

4.5 Limitations

There are several limitations to the work presented in this thesis, most of which have been addressed as they arose, but will be summarized again here. The CMAP recordings from several WT and SOD1^{G93A} mice (not all shown here) stop abruptly at various ages due to the removal of the head cap or the EMG electrode by the mouse which resulted in a smaller number of animals for these experiments. Secondly, the c-fos analysis of $V0_C$ activity during walking and swimming in WT and SOD1^{G93A} mice is purely qualitative and systematic quantification of the number of c-fos positive, ChAT positive neurons in the vicinity of the central canal under each condition needs to be done. Furthermore, the reliability and sensitivity of c-fos for detecting different patterns of neuronal activity during different locomotor tasks was not assessed. Though we qualitatively observed different patterns of c-fos activation in resting, walking, and swimming animals, this observation should be systematically quantified. The most significant limitation of this work was the use of exclusively male SOD1^{G93A} mice for characterizing disease progression. While this was done to avoid gender differences in disease progression in the SOD1^{G93A} line (Herron & Miles, 2012; Veldink et al., 2003), four of the five SOD1;C^{OFF} mice used in this study were female. Although the intention was to also use male SOD1;C^{OFF} mice, the yield of animals that contained *SOD1^{G93A}, Cre* recombinase, and *Chat$^{fl/fl}$* was very low and females had to be added to increase the sample size. Therefore, more male animals should be added to the experiment and comparisons should be made between the male and female data to determine whether there are any significant gender differences. Another limitation of this study was the lack of WT;C^{OFF} mice, especially for the gait parameters and maximal treadmill speed. We show using c-fos immunohistochemistry that C-boutons are not active in WT mice during walking at 0.2m/s and it is therefore unlikely that silencing the C-boutons would cause gait or speed deficits. However, it is not known whether C-

boutons are active at higher speeds which could have implications for the maximal treadmill speed data. We have preliminarily addressed this issue (data not shown), and both of the WT;C^{OFF} mice that we have assessed are capable of walking on the treadmill at 0.5m/s from P80-P120. Nevertheless, more animals at a broader age range should be added to this data.

4.6 Future Directions

Future work should address the limitations that have been outlined regarding the number of animals, quantification of data, and the addition of more male animals to the SOD1;C^{OFF} experiments. Additionally, it would be interesting to perform the CMAP experiments on the SOD1;C^{OFF} mice to elucidate whether C-bouton modulation of motor neurons causes changes in the onset and rate of progression of motor unit loss in $SOD1^{G93A}$ mice. Previous reports have highlighted the potential for C-bouton modulation of motor neurons to lead to excitotoxic motor neuron degeneration (Herron & Miles, 2012; Witts et al., 2014). Although our limited data show that $SOD1^{G93A}$ mice and SOD1;C^{OFF} mice reach humane end-points at similar ages, a more detailed analysis of motor unit changes would allow for more direct conclusions regarding the long-term consequences of C-bouton modulation in ALS. Future experiments should also assess the efficacy of different therapies for improving motor function. Treatment groups could involve a treadmill walking group, a swimming group, a nerve stimulation group and a pharmacologically treated group to assess how different levels of muscle activation contribute to recovery or preservation of motor function as assessed by changes in gait.

4.7 Conclusion

ALS is a relentlessly progressive neurodegenerative disease that causes muscle weakness, paralysis, and eventually death due to motor unit loss. Compensation for motor unit loss is known to occur in ALS patients and mouse models of the disease, yet remarkably little is known about the mechanism. The results presented in this thesis provide evidence that compensation is accomplished, at least in part, by increasing the excitability of motor neurons through C-bouton modulation. We showed that $V0_C$ interneurons, the neuronal source of C-boutons, are active in $SOD1^{G93A}$ mice at ages when significant denervation has occurred. Furthermore, when we silenced the C-boutons in $SOD1^{G93A}$ mice, motor behaviour abnormalities were detected ~15-20 days earlier than in $SOD1^{G93A}$ mice with functional C-boutons. Understanding the motor system's natural compensatory mechanism has significant therapeutic implications. Based on our observations that C-bouton modulation is involved in compensation, treatments that specifically target and upregulate C-bouton activity, whether through exercise or pharmacology, can be developed. Through the development of more efficient therapies, the mobility and quality of life of ALS patients can be improved.

References

Akay, T. (2014). Long-term measurement of muscle denervation and locomotor behavior in individual wild-type and ALS model mice. *Journal of Neurophysiology*, *111*(3), 694–703. http://doi.org/10.1152/jn.00507.2013

Akay, T., Acharya, H. J., Fouad, K., Pearson, K. G., Akay, T., Acharya, H. J., … Keir, G. (2006). Behavioral and Electromyographic Characterization of Mice Lacking EphA4 Receptors Behavioral and Electromyographic Characterization of Mice Lacking EphA4 Receptors. *Journal of Neurophysiology*, *96*(2), 642–651. http://doi.org/10.1152/jn.00174.2006

Akay, T., Tourtellotte, W. G., Arber, S., & Jessell, T. M. (2014). Degradation of mouse locomotor pattern in the absence of proprioceptive sensory feedback. *Proceedings of the National Academy of Sciences of the United States of America*, *111*(47), 16877–16882. http://doi.org/10.1073/pnas.1419045111

Atkin, J. D., Scott, R. L., West, J. M., Lopes, E., Quah, A. K. J., & Cheema, S. S. (2005). Properties of slow- and fast-twitch muscle fibres in a mouse model of amyotrophic lateral sclerosis. *Neuromuscular Disorders*, *15*, 377–388. http://doi.org/10.1016/j.nmd.2005.02.005

Bansal, M., Singhvi, I. J., & Rajpurohit, R. (2015). AMYOTROPHIC LATERAL SCLEROSIS : A REVIEW. *International Journal of Medicine & Health Research*, *1*(1), 1–5.

Boillée, S., Yamanaka, K., Lobsiger, C. S., Copeland, N. G., Jenkins, N. A., Kassiotis, G., … Cleveland, D. W. (2006). Onset and Progression in Inherited ALS Determined by Motor Neurons and Microglia. *Science*, *312*(5778), 1389–1392.

Burke, R. E. (1967). MOTOR UNIT TYPES OF CAT TRICEPS SURAE MUSCLE. *Journal of Physiology*, *193*, 141–160.

Burke, R. E. (1980). Motor unit types: functional specializations in motor control. *Trends in Neurosciences*, *3*(11), 255–258. http://doi.org/10.1016/0166-2236(80)90095-8

Burke, R. E., Levine, D. N., Tsairis, P., & Zajac III, F. E. (1973). Physiological types and histochemical profiles in motor units of the cat gastrocnemius. *The Journal of Physiology*, *234*(3), 723–48. Retrieved from http://www.ncbi.nlm.nih.gov/pubmed/4148752

Burke, R. E., Levine, D. N., Zajac, F. E., Tsairis, P., & Engel, W. K. (1971). Mammalian Motor Units: Physiological-Histochemical Correlation in Three Types in Cat Gastrocnemius. *Science*, *174*(4010), 709–712. Retrieved from http://www.jstor.org/stable/1733761

Chang, Q., & Martin, L. J. (2009). Glycinergic Innervation of Motoneurons Is Deficient in Amyotrophic Lateral Sclerosis Mice: A Quantitative Confocal Analysis. *The American Journal of Pathology*, *174*(2), 574–585. http://doi.org/10.2353/ajpath.2009.080557

Chiu, A. Y., Zhai, P., Dal Canto, M. C., Peters, T. M., Kwon, Y. W., Prattis, S. M., & Gurney, M. E. (1995). Age-Dependent Penetrance of Disease in a Transgenic Mouse Model of Familial Amyotrophic Lateral Sclerosis. *Molecular and Cellular Neuroscience*, *6*, 349–362.

Cleveland, D. W., & Rothstein, J. D. (2001). From Charcot to Lou Gehrig: deciphering selective motor neuron death in ALS. *Nature Reviews. Neuroscience*, *2*(11), 806–819. http://doi.org/10.1038/35097565

Conradi, S., & Skoglund, S. (1960). Observations on the ultrastructure and distribution of neuronal and glial elements on the motoneuron surface in the lumbosacral spinal cord of the cat during postnatal development. *Acta Physiol Scand Suppl*, *333*(5), 5–52.

Courtine, G., Song, B., Roy, R. R., Zhong, H., Herrmann, J. E., Ao, Y., … Sofroniew, M. V. (2008). Recovery of supraspinal control of stepping via indirect propriospinal relay connections after spinal cord injury. *Nature Medicine*, *14*(1), 69–74. http://doi.org/10.1038/nm1682

Dal Bello-Haas, V. P. M., Florence, J. M., Kloos, A. D., Scheirbecker, J., Lopate, G., Hayes, S. M., … Mitsumoto, H. (2007). A Randomized Controlled Trial of Resistance Exercise in Individuals With Als. *Neurology*, *68*(23), 2003–2007. http://doi.org/10.1212/01.wnl.0000327290.13342.0a

Deardorff, A. S., Romer, S. H., Deng, Z., Bullinger, K. L., Nardelli, P., Cope, T. C., & Fyffe, R. E. W. (2013). Expression of postsynaptic Ca2+-activated K+ (SK) channels at C-bouton synapses in mammalian lumbar α-motoneurons. *The Journal of Physiology*, *591*(4), 875–897. http://doi.org/10.1113/jphysiol.2012.240879

Di Giorgio, F. P., Carrasco, M. A., Siao, M. C., Maniatis, T., & Eggan, K. (2007). Non-cell autonomous effect of glia on motor neurons in an embryonic stem cell-based ALS model. *Nature Neuroscience*, *10*(5), 608–614. http://doi.org/10.1038/nn1885

Drory, V. E., Goltsman, E., Goldman Reznik, J., Mosek, A., & Korczyn, A. D. (2001). The value of muscle exercise in patients with amyotrophic lateral sclerosis. *Journal of the Neurological Sciences*, *191*, 133–137. Retrieved from www.elsevier.comrlocaterjns

Edstrom, L., & Kugelberg, E. (1968). Histochemical composition, distribution of fibres and fatiguability of single motor units. *Journal of Neurology, Neurosurgery, and Psychiatry*, *31*(5), 424–433.

Fischer, L. R., Culver, D. G., Tennant, P., Davis, A. A., Wang, M., Castellano-Sanchez, A., … Glass, J. D. (2004). Amyotrophic lateral sclerosis is a distal axonopathy: Evidence in mice and man. *Experimental Neurology*, *185*(2), 232–240. http://doi.org/10.1016/j.expneurol.2003.10.004

Frey, D., Schneider, C., Xu, L., Borg, J., Spooren, W., & Caroni, P. (2000). Early and selective loss of neuromuscular synapse subtypes with low sprouting competence in motoneuron diseases. *The Journal of Neuroscience : The Official Journal of the Society for Neuroscience*, *20*(7), 2534–42. Retrieved from http://www.ncbi.nlm.nih.gov/pubmed/10729333

Gerber, Y. N., Sabourin, J.-C., Rabano, M., Vivanco, M. dM, & Perrin, F. E. (2012). Early Functional Deficit and Microglial Disturbances in a Mouse Model of Amyotrophic Lateral Sclerosis. *PLoS ONE*, *7*(4), 1–11. http://doi.org/10.1371/journal.pone.0036000

Gould, T. W., Buss, R. R., Vinsant, S., Prevette, D., Sun, W., Knudson, C. M., … Oppenheim, R. W. (2006). Complete Dissociation of Motor Neuron Death from Motor Dysfunction by Bax Deletion in a Mouse Model of ALS. *Journal of Neuroscience*, *26*(34), 8774–8786. http://doi.org/10.1523/JNEUROSCI.2315-06.2006

Grillner, S. (1975). Locomotion in vertebrates: central mechanisms and reflex interaction. *Physiological Reviews*, *55*(2), 247–304. http://doi.org/10.1007/978-1-4757-0964-3_18

Guillot, T. S., Asress, S. A., Richardson, J. R., Glass, J. D., & Miller, G. W. (2008). Treadmill Gait Analysis Does Not Detect Motor Deficits in Animal Models of Parkinson's Disease or Amyotrophic Lateral Sclerosis. *Journal of Motor Behavior*, *40*(6), 568–577. http://doi.org/10.3200/JMBR.40.6.568-577

Gurney, M. E., Pu, H., Chiu, A. Y., Dal Canto, M. C., Polchow, C. Y., Alexander, D. D., … Siddique, T. (1994). Motor Neuron Degeneration in Mice That Express a Human Cu,Zn Superoxide Dismutase Mutation. *Science*, *264*, 1772–1775.

Hegedus, J., Putman, C. T., & Gordon, T. (2007). Time course of preferential motor unit loss in the SOD1G93A mouse model of amyotrophic lateral sclerosis. *Neurobiology of Disease*, *28*(2), 154–164. http://doi.org/10.1016/j.nbd.2007.07.003

Hellström, J., Oliveira, A. L. R., Meister, B., & Cullheim, S. (2003). Large cholinergic nerve terminals on subsets of motoneurons and their relation to muscarinic receptor type 2. *Journal of Comparative Neurology*, *460*(4), 476–486. http://doi.org/10.1002/cne.10648

Henneman, E. (1957). Relation between Size of Neurons and Their Susceptibility to Discharge. *Science*, *126*(3287), 1345–1347. Retrieved from http://www.jstor.org/stable/1752769

Herron, L. R., & Miles, G. B. (2012). Gender-specific perturbations in modulatory inputs to motoneurons in a mouse model of amyotrophic lateral sclerosis. *Neuroscience*, *226*, 313–323. http://doi.org/10.1016/j.neuroscience.2012.09.031

Huang, A., Noga, B. R., Carr, P. A., Fedirchuk, B., & Jordan, L. M. (2000). Spinal Cholinergic Neurons Activated During Locomotion: Localization and Electrophysiological Characterization. *Journal of Neurophysiology*, *83*(6), 3537–3547.

Hutchison, D. L., Roy, R. R., Hodgson, J. A., & Edgerton, V. R. (1989). EMG amplitude relationships between the rat soleus and medial gastrocnemius during various motor tasks. *Brain Research*, *502*(2), 233–244. http://doi.org/10.1016/0006-8993(89)90618-5

Kanning, K. C., Kaplan, A., & Henderson, C. E. (2010). Motor Neuron Diversity in Development and Disease. *Annual Review of Neuroscience*, *33*, 409–440. http://doi.org/10.1146/annurev.neuro.051508.135722

Kaspar, B. K., Frost, L. M., Christian, L., Umapathi, P., & Gage, F. H. (2005). Synergy of insulin-like growth factor-1 and exercise in amyotrophic lateral sclerosis. *Annals of Neurology*, *57*(5), 649–655. http://doi.org/10.1002/ana.20451

Kiernan, M. C., Vucic, S., Cheah, B. C., Turner, M. R., Eisen, A., Hardiman, O., … Zoing, M. C. (2011). Amyotrophic lateral sclerosis. *The Lancet*, *377*(9769), 942–955. http://doi.org/10.1016/S0140-6736(10)61156-7

Kirkinezos, I. G., Hernandez, D., Bradley, W. G., & Moraes, C. T. (2003). Regular exercise is beneficial to a mouse model of amyotrophic lateral sclerosis. *Annals of Neurology*, *53*(6), 804–807. http://doi.org/10.1002/ana.10597

Lasiene, J., Komine, O., Fujimori-Tonou, N., Powers, B., Endo, F., Watanabe, S., … Yamanaka, K. (2016). Neuregulin 1 confers neuroprotection in SOD1-linked amyotrophic lateral sclerosis mice via restoration of C-boutons of spinal motor neurons. *Acta Neuropathologica Communications*, *4*(15), 1–13. http://doi.org/10.1186/s40478-016-0286-7

Leblond, H., L ’Espérance, M., Orsal, D., & Rossignol, S. (2003). Treadmill Locomotion in the Intact and Spinal Mouse. *J. Neurosci.*, *23*(36), 11411–19.

Maathuis, E. M., Drenthen, J., Van Doorn, P. A., Visser, G. H., & Blok, J. H. (2013). The CMAP Scan as a Tool to Monitor Disease Progression in ALS and PMA. *Amyotrophic Lateral Sclerosis and Frontotemporal Degeneration*, *14*, 217–223. http://doi.org/10.3109/21678421.2012.732079

Mahoney, D. J., Rodriguez, C., Devries, M., Yasuda, N., & Tarnopolsky, M. A. (2004). Effects of high-intensity endurance exercise training in the G93A mouse model of amyotrophic lateral sclerosis. *Muscle & Nerve*, *29*(5), 656–662. http://doi.org/10.1002/mus.20004

Major, L. A., Hegedus, J., Weber, D. J., Gordon, T., & Jones, K. E. (2007). Method for Counting Motor Units in Mice and Validation Using a Mathematical Model. *Journal of Neurophysiology*, *97*(2), 1846–1856. http://doi.org/10.1152/jn.00904.2006

Mancuso, R., Oliván, S., Osta, R., & Navarro, X. (2011). Evolution of gait abnormalities in SOD1 G93A transgenic mice. *Brain Research*, *1406*, 65–73. http://doi.org/10.1016/j.brainres.2011.06.033

McComas, A. ., Sica, R. E. ., Campbell, M. ., & Upton, A. . (1971). Functional compensation in partially denervated muscles. *Journal of Neurology, Neurosurgery, and Psychiatry*, *34*(4), 453–460. http://doi.org/10.1136/JNNP.34.4.453

Mead, R. J., Bennett, E. J., Kennerley, A. J., Sharp, P., Sunyach, C., Kasher, P., … Shaw, P. J. (2011). Optimised and Rapid Pre-clinical Screening in the SOD1 G93A Transgenic Mouse Model of Amyotrophic Lateral Sclerosis (ALS). *PLoS One*, *6*(8), 1–12. http://doi.org/10.1371/journal.pone.0023244

Milan, L., Courtand, G., Cardoit, L., Masmejean, F., Barrière, G., Cazalets, J.-R., … Wolpaw, J. (2015). Age-Related Changes in Pre- and Postsynaptic Partners of the Cholinergic C-Boutons in Wild-Type and SOD1G93A Lumbar Motoneurons. *PLoS ONE*, *10*(8), e0135525. http://doi.org/10.1371/journal.pone.0135525

Miles, G. B., Hartley, R., Todd, A. J., & Brownstone, R. M. (2007). Spinal cholinergic interneurons regulate the excitability of motoneurons during locomotion. *Proceedings of the National Academy of Sciences of the United States of America*, *104*(7), 2448–2453. http://doi.org/10.1073/pnas.0611134104

Nagai, M., Re, D. B., Nagata, T., Chalazonitis, A., Jessell, T. M., Wichterle, H., & Przedborski, S. (2007). Astrocytes expressing ALS-linked mutated SOD1 release factors selectively toxic to motor neurons. *Nature Neuroscience*, *10*(5), 615–622. http://doi.org/10.1038/nn1876

Nagao, M., Misawa, H., Kato, S., & Hirai, S. (1998). Loss of cholinergic synapses on the spinal motor neurons of amyotrophic lateral sclerosis. *Journal of Neuropathology and Experimental Neurology*, *57*(4), 329–333. Retrieved from http://jnen.oxfordjournals.org/

Nardo, G., Trolese, M. C., Tortarolo, M., Vallarola, A., Freschi, M., Pasetto, L., … Bendotti, C. (2016). New Insights on the Mechanisms of Disease Course Variability in ALS from Mutant SOD1 Mouse Models. *Brain Pathology*, *26*, 237–247. http://doi.org/10.1111/bpa.12351

Pasinelli, P., & Brown, R. H. (2006). Molecular biology of amyotrophic lateral sclerosis : insights from genetics, *7*(September), 18–23. http://doi.org/10.1038/nrn1971

Pearson, K. G., Acharya, H., & Fouad, K. (2005). A new electrode configuration for recording electromyographic activity in behaving mice. *Journal of Neuroscience Methods*, *148*(1), 36–42. http://doi.org/10.1016/j.jneumeth.2005.04.006

Pinto, A. C., Alves, M., Nogueira, A., Evangelista, T., Carvalho, J., Coelho, A., … Lurdes Sales-Luıs, M. (1999). Can amyotrophic lateral sclerosis patients with respiratory insufficiency exercise? *Journal of the Neurological Sciences*, *169*, 69–75. Retrieved from www.elsevier.com

Preisig, D. F., Kulic, L., Krüger, M., Wirth, F., McAfoose, J., Späni, C., … Welt, T. (2016). High-speed video gait analysis reveals early and characteristic locomotor phenotypes in mouse models of neurodegenerative movement disorders. *Behavioural Brain Research*, *311*, 340–353. http://doi.org/10.1016/j.bbr.2016.04.044

Pullen, A. H., & Athanasiou, D. (2009). Increase in presynaptic territory of C-terminals on lumbar motoneurons of G93A SOD1 mice during disease progression. *European Journal of Neuroscience*, *29*(3), 551–561. Retrieved from http://web.a.ebscohost.com.ezproxy.library.dal.ca/ehost/pdfviewer/pdfviewer?sid=51535c60-f673-4e4c-84f6-4ff034088664%40sessionmgr4008&vid=1&hid=4104

Pun, S., Santos, A. F., Saxena, S., Xu, L., & Caroni, P. (2006). Selective vulnerability and pruning of phasic motoneuron axons in motoneuron disease alleviated by CNTF. *Nature Neuroscience*, *9*(3), 408–419. http://doi.org/10.1038/nn1653

Robberecht, W., & Philips, T. (2013). The changing scene of amyotrophic lateral sclerosis. *Nature Reviews. Neuroscience*, *14*(4), 248–64. http://doi.org/10.1038/nrn3430

Sanes, J. R., & Lichtman, J. W. (1999). Development of the Vertebrate Neuromuscular Junction. *Annu. Rev. Neurosci*, *22*, 389–442.

Saxena, S., Roselli, F., Singh, K., Leptien, K., Julien, J.-P., Gros-Louis, F., & Caroni, P. (2013). Neuroprotection through Excitability and mTOR Required in ALS Motoneurons to Delay Disease and Extend Survival. *Neuron*, *80*(1), 80–96. http://doi.org/10.1016/j.neuron.2013.07.027

Schaefer, A. M., Sanes, J. R., & Lichtman, J. W. (2005). A compensatory subpopulation of motor neurons in a mouse model of amyotrophic lateral sclerosis. *The Journal of Comparative Neurology*, *490*(3), 209–219. http://doi.org/10.1002/cne.20620

Tysseling, V. M., Janes, L., Imhoff, R., Quinlan, K. A., Lookabaugh, B., Ramalingam, S., … Tresch, M. C. (2013). Design and evaluation of a chronic EMG multichannel detection system for long-term recordings of hindlimb muscles in behaving mice. *Journal of Electromyography and Kinesiology*, *23*, 531–539. http://doi.org/10.1016/j.jelekin.2012.11.014

van Dijk, J. P., Schelhaas, H. J., Van Schaik, I. N., Janssen, H. M. H. A., Stegeman, D. F., & Zwarts, M. J. (2010). Monitoring disease progression using high-density motor unit number estimation in amyotrophic lateral sclerosis. *Muscle & Nerve*, *42*(2), 239–244. http://doi.org/10.1002/mus.21680

Veldink, J. H., Bär, P. R., Joosten, E. A. J., Otten, M., Wokke, J. H. J., & van den Berg, L. H. (2003). Sexual differences in onset of disease and response to exercise in a transgenic model of ALS. *Neuromuscular Disorders*, *13*(9), 737–743. http://doi.org/10.1016/S0960-8966(03)00104-4

Vinsant, S., Mansfield, C., Jimenez-Moreno, R., Del, V., Moore, G., Yoshikawa, M., … Milligan, C. (2013). Characterization of early pathogenesis in the SOD1 G93A mouse model of ALS: part I, background and methods. *Brain and Behavior*, *3*(4), 335–350. http://doi.org/10.1002/brb3.143

Vinsant, S., Mansfield, C., Jimenez-Moreno, R., Moore, V. D. G., Yoshikawa, M., Hampton, T. G., … Milligan, C. (2013). Characterization of early pathogenesis in the SOD1G93A mouse model of ALS: Part II, results and discussion. *Brain and Behavior*, *3*(4), 431–457. http://doi.org/10.1002/brb3.142

Winter, D. A. (1990). *Muscle Mechanics*. *Biomechanics and Motor Control of Human Movement*. http://doi.org/10.1002/9780470549148

Witts, E. C., Zagoraiou, L., & Miles, G. B. (2014). Anatomy and function of cholinergic C bouton inputs to motor neurons. *Journal of Anatomy*, *224*(1), 52–60. http://doi.org/10.1111/joa.12063

Wooley, C. M., Sher, R. B., Kale, A., Frankel, W. N., Cox, G. A., & Seburn, K. L. (2005). Gait analysis detects early changes in transgenic SOD1(G93A) mice. *Muscle & Nerve*, *32*(1), 43–50. http://doi.org/10.1002/mus.20228

Zagoraiou, L., Akay, T., Martin, J. F., Brownstone, R. M., Jessell, T. M., & Miles, G. B. (2009). A cluster of cholinergic premotor interneurons modulates mouse locomotor activity. *Neuron*, *64*(5), 645–62. http://doi.org/10.1016/j.neuron.2009.10.017

Zehr, E. P. (2002). Considerations for use of the Hoffmann reflex in exercise studies. *European Journal of Applied Physiology*, *86*(6), 455–468. http://doi.org/10.1007/s00421-002-0577-5